Hokkaido Mathematical Journal Vol. 36 (2007) p. 207–242

Dynamics of traveling pulses in heterogeneous media of jump type

Yasumasa NISHIURA, Yoshihito OYAMA and Kei-ichi UEDA

(Received December 7, 2005; Revised June 15, 2006)

Abstract. We study pulse dynamics in one-dimensional heterogeneous media. In particular we focus on the case where the pulse is close to the singularity of codim 2 type consisting of drift and saddle-node instabilities in a parameter space. We assume that the heterogeneity is of jump type, namely one of the coefficients of the system undergoes an abrupt change at one point in the space. Depending on the height of this jump, the responses of pulse behavior are penetration, splitting, and rebound. Taking advantage of the fact that pulse is close to the singularity, the PDE dynamics can be reduced to a finite-dimensional system, which displays the three behaviors. Moreover it takes a universal form independent of model systems, and is valid for much more general heterogeneities such as bump, periodic, and random cases.

Key words: reaction-diffusion equations (35K57), Bifurcation (35B32), Homoclinic and Heteroclinic solutions (34C37).

1. Introduction

Spatially localized patterns such as pulses and spots are fundamental objects arising in many dissipative systems such as [1, 3, 4, 14, 19, 26, 35]. One of the recent remarkable discoveries is that there is a class of localized patterns which display a variety of dynamics such as elastic ball-like behaviors upon collision, self-replication, self-destruction and spatiotemporal chaos [2, 5, 7, 12, 17, 20, 22, 23, 24, 27, 33, 34, 36, 39]. This makes a sharp contrast with the well-known classical excitable waves as in the FitzHugh-Nagumo (FHN) equations in which annihilation are typically observed when they collide with others [16].

One of the origins of such rich behaviors is that the pulses have their own internal dynamics; namely, they have a variety of instabilities depending on parameters. For instance, saddle-node structure causes self-replication [21], and drift bifurcation is responsible for the onset of traveling motion. Moreover a singularity of codim 2 type, i.e., a system has a parameter where multiple bifurcations simultaneously occur, is known to be responsible for

2000 Mathematics Subject Classification : 35K57, 35B32, 34C37.

the variety of outputs for scattering process [22, 25]. The pulses treated here in this paper are asymptotically stable in homogeneous media, however we assume that the associated parameter values are located close to the above instabilities. One of the consequences of this assumption is the enhancement of sensitivity to the perturbation: for instance, if the associated parameter with traveling pulse is close to the drift bifurcation, its profile is almost symmetric and easy to deform from the right-going pulse to the left-going one due to the external perturbations, which is one of the characteristic differences between FHN pulses and ours.

Behavior of such pulses or spots in heterogeneous media are not so well-studied compared with the FHN pulses [10, 11, 28, 29] and the front case [6, 13, 15, 38]. The aim of this paper is to show how one-dimensional stable traveling pulses in such a class behave when there exists a spatial heterogeneity in the media. Here we restrict ourselves to the simplest case in which there is only one Heaviside-like abrupt change of a parameter value which may affect the propagating manner. We will briefly discuss the bump (two abrupt changes) and periodic cases in the concluding remarks.

To be specific, we employ two model systems: one is the Gray-Scott model (1) and the other is the exothermic model (2) (see Section 2) and consider the case in which one of the kinetic parameters (k for (1) or b for (2)) changes abruptly around a point. Although we mainly deal with the Gray-Scott model in this paper, the method employed here is also applicable to many other systems including the exothermic model syetem. Fig. 1 schematically illustrates a traveling pulse in a heterogeneous medium, in which the kinetic parameter varies like a smoothed Heaviside-like function so that the propagation velocity in the right-half region is lower than that in the left-half region. It is in a sense that the pulse goes into a bad environment.

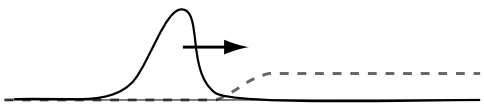

Fig. 1. The solid line shows a profile traveling pulse schematically. The dotted line stands for the typical profile of parameter $k = k(x)$ in our model system. Traveling pulses meet the heterogeneity $k(x)$ of jump type in the middle. For the Gray-Scott model we observe three different responses shown in Fig. 2

It is the case, in fact, if the parameter (k for (1) or b for (2)) is increased as x exceeds the jump point. One may expect that pulses can go through the jump point when the height is very low. However, it is not so clear for higher barriers whether the pulse turns back, annihilates or splits into two waves, in fact, it turns out that penetration does not always occur even for arbitrary small jump when other parameters are tuned appropriately. Fig. 2 shows three different responses for the Gray-Scott model (3) when the pulse meets a heterogeneity of jump type in the middle. For small gap, the pulse can penetrate into the right-half region. When the size of gap is gradually increased, the pulse splits around the jump point, and then it turns back. Note that the splitting of the pulse can occur without the heterogeneous effect, i.e., spontaneous splitting as in Fig. 4 due to intrinsic instability of saddle-node type in which stable traveling pulses are not observable. Here we are interested in the situation that pulses can propa-

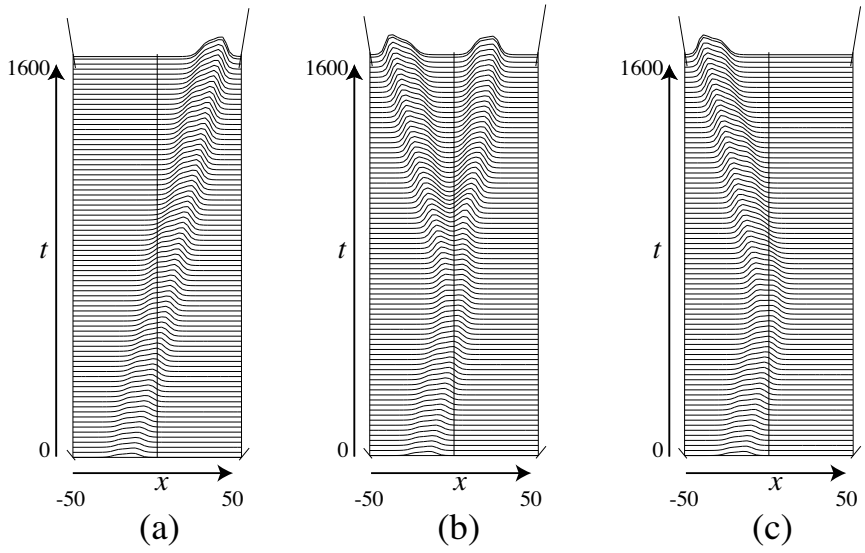

Fig. 2. Heterogeneity causes a variety of pulse dynamics as its height ϵ varies. (a) Penetration ($f = 0.026$, $k = 0.0557$, $\epsilon = 2.0 \times 10^{-4}$), (b) Splitting ($f = 0.026$, $k = 0.0557$, $\epsilon = 7.0 \times 10^{-4}$), (c) Rebound ($f = 0.026$, $k = 0.0557$, $\epsilon = 1.2 \times 10^{-3}$). The coefficient $k(x)$ for the Gray-Scott model (3) has a heterogeneity of jump type located at the center of the interval as in Fig. 1. The computations are carried out for $\Delta t = 0.05$, $-50 \leq x \leq 50$ and $\Delta x = 0.125$.

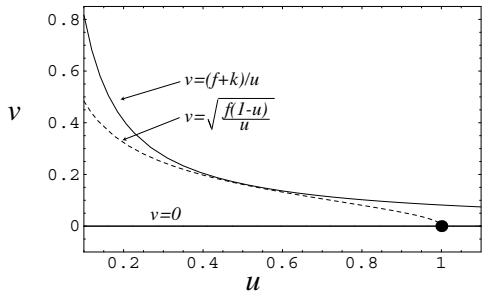

Fig. 3. The Gray-Scott model (1) has only one homogeneous state $(u, v) = (1, 0)$ in our paper. Two nullclines $v = (f + k)/u$ and $v = \sqrt{f(1-u)/u}$ for $f = 0.026$ and $k = 0.0557$ do not intersect.

gate stably on both sides of the jump point and splitting is caused by the heterogeneity and occurs only once around the jump point.

One of our main goals is to explain the reduction from PDE dynamics to ODE ones via pulse interaction method [5, 7, 8], and then clarify the role of the codim 2 singularity consisting of the drift bifurcation and the saddle-node bifurcation, which leads to the origin of various responses due to the heterogeneity. The drift bifurcation is a deformation of wave form of symmetry-breaking type which drives a standing pulse into a moving one and the saddle-node bifurcation causes a sudden onset of an event such as wave-splitting as in Fig. 4.

A remarkable thing is that the resulting finite dimensional dynamics not only inherit the qualitative aspect of the original PDE dynamics but also is independent of specific model systems and valid for much more general heterogeneity including periodic and random cases.

This paper consists of 6 Sections. The model system and its properties in homogeneous media are shown in Section 2. Section 3 numerically shows pulse behaviors in heterogeneous media. Section 4 presents the reduction to finite-dimensional dynamics. In Section 5 we discuss the analysis of the principal part of the reduced equations. And then, we conclude our discussions in Section 6.

2. Model systems

We consider the following one-dimensional reaction-diffusion system called the Gray-Scott model [9, 30], which describes the chemical reaction

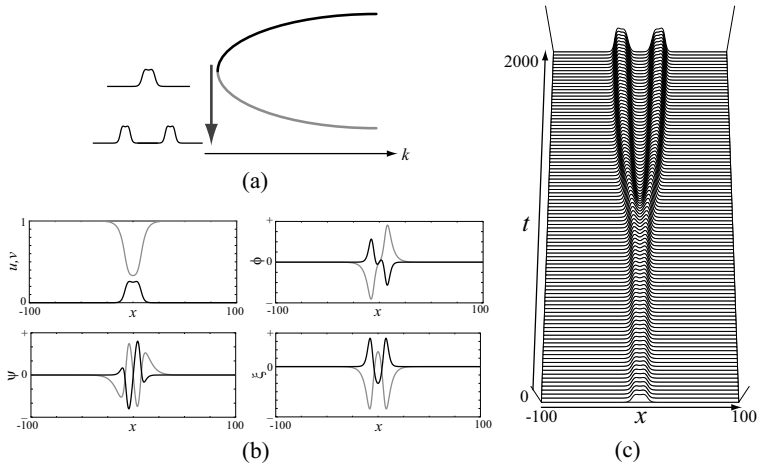

Fig. 4. The saddle-node bifurcation of standing pulse for the Gray-Scott model. Fig. (a) shows a schematic picture of flows near the saddle-node bifurcation point. Here the black (gray) line indicates stable (unstable) standing pulse solution. The unstable manifold emanating from the lower (gray) branch of saddle-node bifurcation is responsible for the splitting from 1-pulse to 2-pulse type of solutions. Figures in (b) show the profile of standing pulse at codim 2 point (left up) and the associated eigenfunctions: ϕ for translation free zero eigenvalue (right up), ψ for drift bifurcation (left bottom), and ξ for saddle-node one (right bottom) respectively ($k \approx 0.057833$, $\tau \approx 1.007734$, $f = 0.0291$). The black (gray) line indicates the v-component (u-component). The space-time plot (c) shows a pulse-splitting of the standing pulse slightly off the saddle-node bifurcation located at $k = 0.0578$.

$U + 2V \to 3V$ and $V \to P$ in a gel reactor:

$$\begin{cases} \dfrac{\partial u}{\partial t} = D_u \dfrac{\partial^2 u}{\partial x^2} - uv^2 + f(1-u), \\ \tau \dfrac{\partial v}{\partial t} = D_v \dfrac{\partial^2 v}{\partial x^2} + uv^2 - (f+k)v, \end{cases} \quad t > 0,\ x \in \mathbb{R}, \tag{1}$$

where $u = u(t, x)$ and $v = v(t, x)$ depend on time t and position x, $f > 0$ and $k > 0$ are kinetic parameters, and $D_u > 0$, $D_v > 0$ and τ are constants. We assume that k is spatially uniform in this section. Since we study the behavior of traveling pulse, we employ the parameter values so that (1) becomes mono-stable, namely the nullclines intersect at only one point

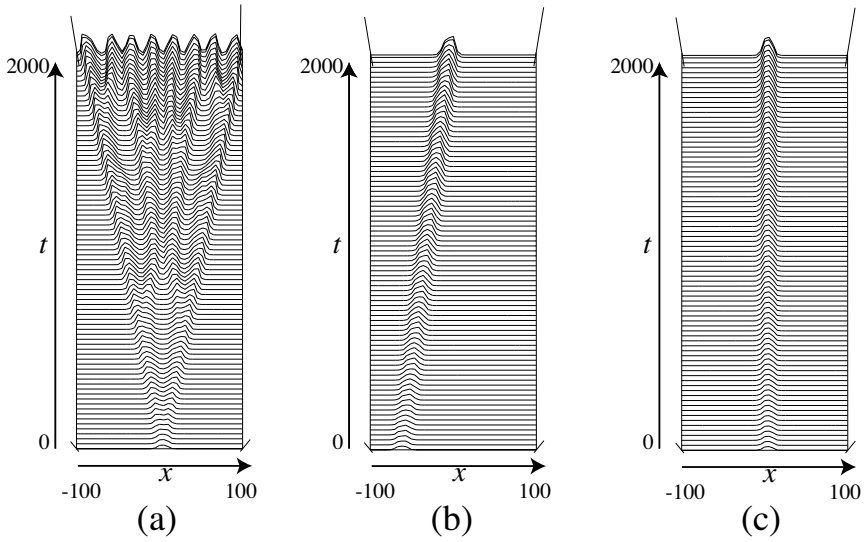

Fig. 5. Dynamics of the Gray-Scott model(1) in homogeneous media when k is increased with $f = 0.026$ being fixed. Computations are done for $\Delta t = 0.05$ and $\Delta x = 0.25$. (a) Splitting pulse ($k = 0.0550$), (b) Traveling pulse ($k = 0.0560$) and (c) Standing pulse ($k = 0.0570$)

(1, 0) (see Fig. 3).

The numerical integration of (1) is carried out with the Crank-Nicholson method [32] with $D_u = 5.0 \times 10^{-1}$, $D_v = 2.5 \times 10^{-1}$, $\tau = 1.007734$, and time interval $\Delta t = 0.05$ with Neumann boundary conditions.

It is known that (1) displays a variety of dynamics [21, 30, 31] depending on k and f. Three different types of pulse dynamics such as splitting, traveling, and standing ones are typically observed as in Fig. 5. The phase diagram in (k, f)-plane is shown in Fig. 6. In Fig. 6, SN (DR)-line denotes the saddle-node (drift) bifurcation of standing pulses, which are numerically computed [32]. The broken line in Fig. 6 separating the splitting domain and traveling one represents the Hopf-bifurcation. The intersection of SN and DR lines is a codim 2 point located at (k, f) $\approx$ (0.057833, 0.0291). The associated eigenfunctions are depicted in Fig. 4 in which ψ represents the main deformation of the drift bifurcation and ξ for the saddle-node one. For $f = 0.026$, the saddle-node bifurcation is at $k = k_{SN} \approx 5.65092 \times 10^{-2}$, the drift bifurcation at $k = k_{DR} \approx 5.65746 \times 10^{-2}$, splitting of traveling pulses occurs in the region of $k \leq k_H \approx 0.05543$, and stable traveling pulses

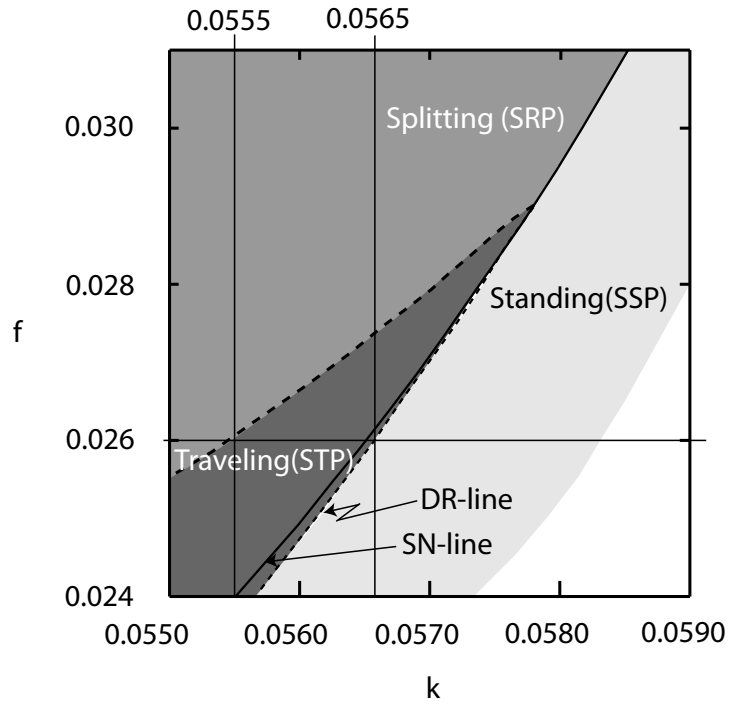

Fig. 6. Phase diagram in (k, f)-plane for the Gray-Scott model (1). Here DR stands for the drift-bifurcation, and SN for the saddle-node one of standing pulses, respectively. The boundary separating the splitting and traveling domains is Hopf bifurcation line of traveling pulses. The crossing point of DR-and SN-lines is the codim 2 point.

exist when k belongs to the interval (k_H, k_{DR}). Standing pulses cease to exist around $k \approx 0.05833$, and only the trivial state $(1, 0)$ is observable asymptotically for $k > 0.05833$.

Before discussing the dynamics of traveling pulses in heterogeneous media, we show several properties of them in homogeneous media. It is numerically confirmed as in Fig. 7 that the above drift bifurcation at $k = k_{DR}$ is supercritical, in fact, it is confirmed numerically that the propagation speed is monotonically decreased with respect to k.

In the next section, we work in the parameter regime: $f = 0.026$ and $0.0555 \leq k \leq 0.0565$ in which stable traveling pulses are observed. All the numerical computations hereafter will be done for $f = 0.026$.

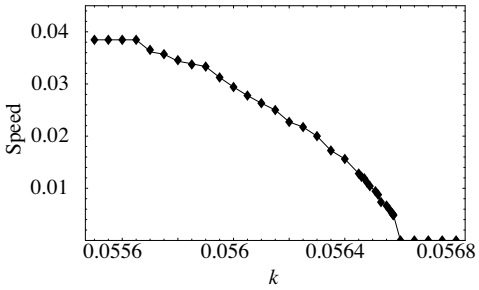

Fig. 7. The propagating speed of the pulse of Gray-Scott system (1) for $f = 0.026$. The drift bifurcation occurs at $k = 0.056574$.

Although we employed (1) as a representative system, our results in sections 4 and 5 have much more generality. In order to illustrate it, we also consider the following reaction-diffusion equations for the exothermic reaction [7]:

$$\begin{cases} \dfrac{\partial u}{\partial t} = \dfrac{\partial^2 u}{\partial x^2} + \kappa^{-1}[-2u + \exp(u/(1+u/5))]v, \\ \dfrac{\partial v}{\partial t} = d\dfrac{\partial^2 v}{\partial x^2} + h(1-v) - \exp(u/(1+u/5))v, \end{cases} \quad t > 0,\ x \in \mathbb{R}, \quad (2)$$

where $u = u(t, x)$ and $v = v(t, x)$ depend on time t and position x, and $h > 0$ is a constant. We numerically integrate this system with $h = 45.0$, and with time step $\Delta t = 1.0 \times 10^{-5}$, using κ and $d > 0$ as control parameters. The system size is 10.0 with $\Delta x = 0.025$. It turns out that this system has a stable stationary pulse (SSP) solution, a self-replication pulse (SRP), i.e., pulse-splitting, a stable traveling pulse (STP) solution, and a stable oscillatory traveling pulse (SOTP) solution. Fig. 8 shows the phase diagram of (2). The codim 2 point, i.e., the intersection of the drift bifurcation (dotted line) and the saddle-node bifurcation (solid line) is located at $(d, \kappa) \approx (5.9105, 0.001027)$. We work in the STP-regime close to the codim 2 point.

3. Pulse dynamics in heterogeneous media

We proceed to study pulse dynamics of the Gray-Scott model (1) and the exothermic model (2) in heterogeneous media.

We introduce a heterogeneity assuming that the parameter k is a func-

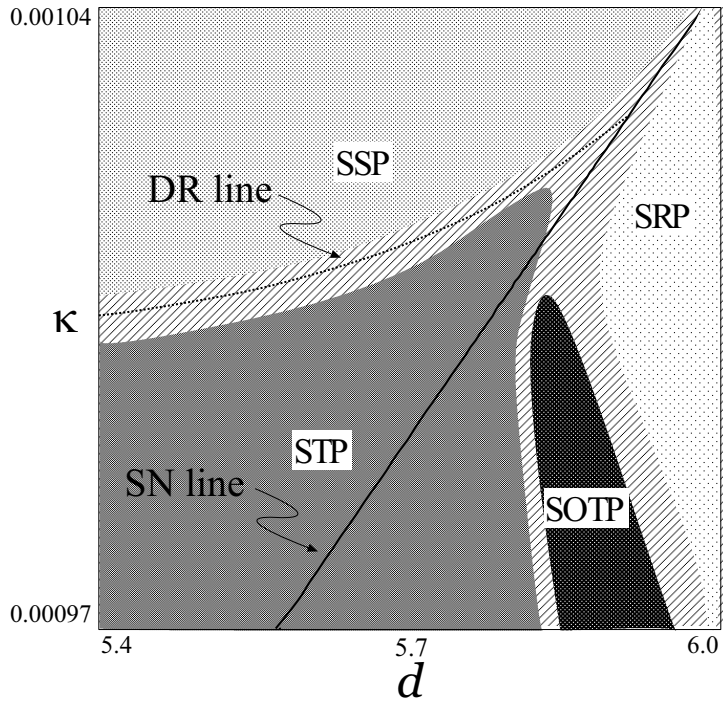

Fig. 8. Phase diagram for the exothermic model (2). Here the regions for stable standing pulse (SSP), self-replication pulse (SRP), stable traveling pulse (STP), and stable oscillatory traveling pulse (SOTP) are shown. DR and SN lines stand for the same bifurcations as in Fig. 6.

tion of x, namely $k(x) = k + \epsilon\chi(x)$,

$$\begin{cases} \dfrac{\partial u}{\partial t} = D_u \dfrac{\partial^2 u}{\partial x^2} - uv^2 + f(1-u), \\ \tau \dfrac{\partial v}{\partial t} = D_v \dfrac{\partial^2 v}{\partial x^2} + uv^2 - (f + k(x))v, \end{cases} \qquad t > 0,\ x \in \mathbb{R}, \tag{3}$$

where $\chi(x) = 1/(1 + \exp(-\gamma x))$ with $\gamma > 0$ as shown in Fig. 9. The parameter ϵ controls the height of the jump and γ controls the slope of the heterogeneity. Jump-up case corresponds to $\epsilon > 0$, jump-down case to $\epsilon < 0$ and $\epsilon = 0$ is a homogeneous case.

We integrate (1) with $k(x)$ given by (3) using the Crank-Nicholson method with $D_u = 5.0 \times 10^{-1}$, $D_v = 2.5 \times 10^{-1}$, $\tau = 1.007734$, $\Delta t = 0.05$, being the same as above for the homogeneous case. We use $f = 0.026$ and

k varies in between 0.05550 and 0.05650, where the stable traveling pulse exists. The steepness of the slope of $k(x)$ around $x = 0$ is controlled by γ, and in fact the response of pulse also depends on γ (see Section 6), however we fix it as $\gamma = 5.0$(see Fig. 9).

Depending on k and the height of the jump ϵ, the response of the pulse can be classified into three classes: penetration, splitting, and rebound as shown in Fig. 10. Loosely speaking, for $\epsilon > 0$ (jump-up), penetration always occurs for lower barriers and rebound is observed for higher barriers. Pulse-splitting occurs in between the above two responses and diminishes as k is increased. Those typical behaviors are depicted in Fig. 2 when ϵ is increased from 2.0×10^{-4} to 1.2×10^{-3}.

The phase-diagram Fig. 10 also shows that penetration (respectively rebound) regime expands as k is decreased (respectively increased). Recall that the velocity of the pulse is increased as k is decreased, and therefore for positive ϵ the pulse propagates faster in the left-side domain than the right-side domain. On the other hand, for $\epsilon < 0$ (jump-down), penetration is always observed.

Next we observe the exothermic model (2) with a heterogeneity via $\kappa(x) = \kappa_0 + \epsilon\chi(x)$:

$$\begin{cases} \dfrac{\partial u}{\partial t} = \dfrac{\partial^2 u}{\partial x^2} - 2\kappa_0^{-1}u + \kappa^{-1}(x)\exp(u/(1+u/5))v, \\ \dfrac{\partial v}{\partial t} = d\dfrac{\partial^2 v}{\partial x^2} + h(1-v) - \exp(u/(1+u/5))v, \end{cases} \quad t > 0,\ x \in \mathbb{R}, \tag{4}$$

where d, h, and κ_0 are constants, and $\chi(x) = 1/(1+\exp(-\gamma x))$ with $\gamma > 0$ is the same as above for $k(x)$ (see (3)). The parameters ϵ and γ respectively control the height of the jump and the slope.

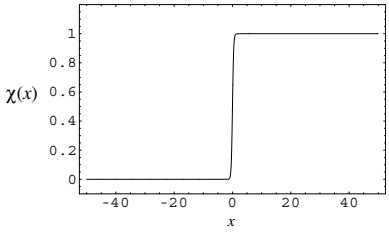

Fig. 9. The profile of $\chi(x)$ for $\gamma = 5.0$.

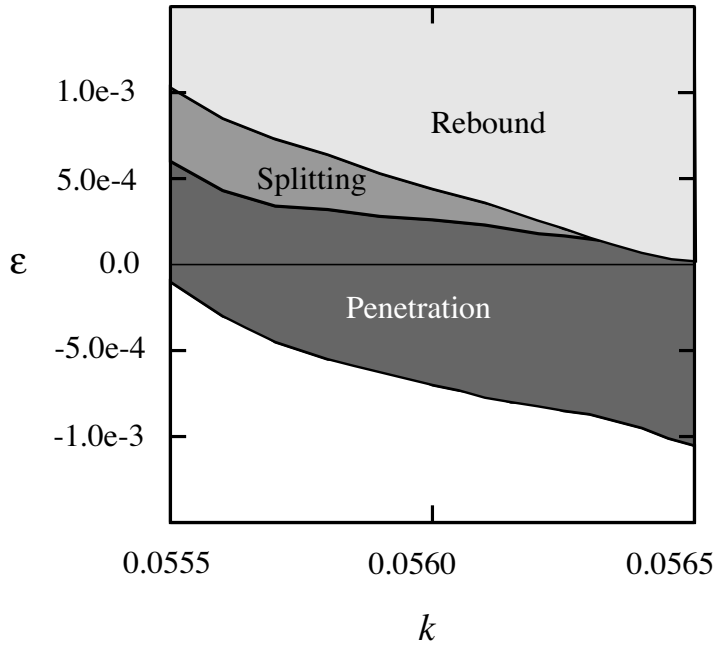

Fig. 10. Response of the pulse in heterogeneous media for the Gray-Scott model with $k(x)$ being given by (3) with respect to k and ϵ.

We integrate (4) with the system size 10.0, spatial interval $\Delta x = 0.025$, and time interval $\Delta t = 1.0 \times 10^{-5}$ for $d = 5.7$, $h = 45.0$, $\kappa_0 = 0.00097$, $\gamma = 5.0$.

Fig. 11 shows the phase diagram of this system, which is qualitatively similar to that for the Gray-Scott model (Fig. 10). When ϵ is increased, the rebound regime appears; there exists a splitting region between the penetration region and the rebound region.

A natural question arises "what is the mathematical mechanism producing the above outputs?" It is known that pulse-splitting is associated with the saddle-node bifurcation as shown in Fig. 4, and the transition from standing to traveling occurs via the drift bifurcation. This suggests that the dynamics of the pulse near the codim 2 singularity consisting of the saddle-node and the drift bifurcation points can give us a clue to understand this variety of responses. In fact, as we will see in the sequel, our reduction method near such codim 2 point produces the expected outputs and allows us to reduce the whole dynamics to a finite-dimensional ODEs

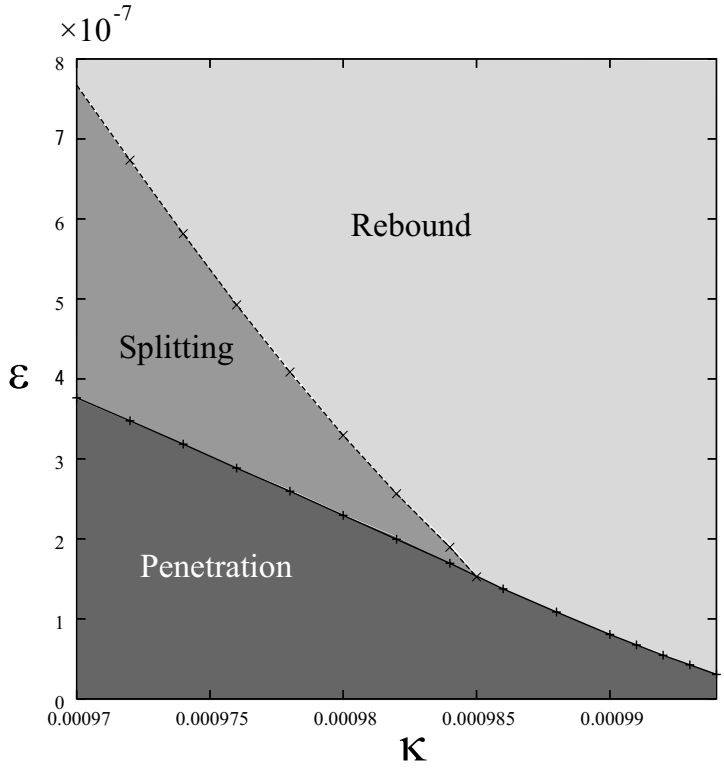

Fig. 11. Response of the pulse in heterogeneous media for the exothermic model (2) with $b(x)$ being given by (4).

which has a universal form independent of specific model systems.

4. Reduction to finite-dimensional dynamics

In order to study the pulse dynamics in heterogeneous media, we analyze the following general 1D reaction-diffusion system

$$\boldsymbol{u}_t = D\boldsymbol{u}_{xx} + F(\boldsymbol{u}; \boldsymbol{k}) =: \mathcal{A}(\boldsymbol{u}; \boldsymbol{k}), \quad t > 0,\ x \in \mathbb{R}, \tag{5}$$

in which parameter $\boldsymbol{k} \in \mathbb{R}^2$ is close to the codim 2 point (see (S3)). Let $X := \{L^2(\mathbb{R})\}^N$, $\boldsymbol{u} = \boldsymbol{u}(t, x) = (u_1, \ldots, u_N)^T \in X$ be an N-dimensional vector, D be a positive diagonal matrix, $F\colon \mathbb{R}^N \to \mathbb{R}^N$ be a smooth vector-valued function, $\boldsymbol{k} = (k_1 + \epsilon\chi(x), k_2)$ with $k_1, k_2, \epsilon \in \mathbb{R}$ and $\chi(x)$ be a C^1-function. For (5), we assume through (S1) to (S4):

(S1) There exists a $\boldsymbol{k} = \boldsymbol{k_c} := (\tilde{k}_1, \tilde{k}_2) \in \mathbb{R}^2$ such that the non-trivial standing pulse solution $S(x; \boldsymbol{k})$ of (5) exists, i.e., $\mathcal{A}(S; \boldsymbol{k_c}) = 0$.

We consider (5) in a neighborhood of $\boldsymbol{k} = \boldsymbol{k_c}$, by using small parameters $\boldsymbol{\eta} = (\eta_1, \eta_2)$ as $k_1 = \tilde{k}_1 + \eta_1$ and $k_2 = \tilde{k}_2 + \eta_2$. In order to avoid the unnecessary complexities, we assume that (5) takes the following form

$$\boldsymbol{u}_t = \mathcal{A}(\boldsymbol{u}; \boldsymbol{k_c}) + (\eta_1 + \epsilon\chi(x))\boldsymbol{g}_1(\boldsymbol{u}) + \eta_2\boldsymbol{g}_2(\boldsymbol{u}),$$

where $\boldsymbol{g}_1$ and $\boldsymbol{g}_2$ are N-dimensional vector-valued functions.

Let L be the linearized operator of $\mathcal{A}$ with respect to $\boldsymbol{u}$ at $\boldsymbol{u} = S$ at $\boldsymbol{k} = \boldsymbol{k}_c$, i.e., $L = \mathcal{A}'(S(x); \boldsymbol{k_c})$, where "$'$" stands for Fréchet derivative with respect to $\boldsymbol{u}$, and L^* be the adjoint operator of L with respect to $\{L^2(\mathbb{R})\}^N$.

(S2) The spectral set of L consists of two sets $\sigma_1 = \{0\}$ and $\sigma_2 \subset \{\mu \in \boldsymbol{C};\ \mathrm{Re}(\mu) < -\gamma_0\}$, where γ_0 is a positive constant.

(S3) L has a codim 2 singularity at $\boldsymbol{k} = \boldsymbol{k_c}$ consisting of drift and saddle-node bifurcations besides the translation-free 0 eigenvalue. That is, there exist three eigenfunctions $\phi(x)$, $\psi(x)$ and $\xi(x)$ such that

$$L\phi = 0, \quad L\psi = -\phi, \quad L\xi = 0,$$

where $\phi = \partial S/\partial x$. Note that $\phi(x)$ and $\psi(x)$ are odd functions, and $\xi(x)$ is an even function. $\psi(x)$ represents the deformation vector with Jordan form for the drift bifurcation, and $\xi(x)$ the eigenfunction for the saddle-node bifurcation.

Similar properties also hold for L^*. That is, there exist ϕ^*, ξ^* and ψ^* such that $L^*\phi = L^*\xi^* = 0$ and $L^*\psi^* = -\phi^*$, where $\phi^*(x)$ and $\psi^*(x)$ are odd functions and $\xi^*(x)$ is an even function.

(S4) Each element of eigenfunctions ϕ, ϕ^*, ψ, ψ^*, ξ, and ξ^* decays exponentially as $|x| \to +\infty$.

The above assumptions are numerically confirmed for (1), in fact Fig. 12 shows the profiles of associated adjoint eigenfunctions at the codim 2 point for the Gray-Scott model.

Remark 4.1 Under the normalization of

$$\langle\psi, \phi\rangle = \langle\psi, \psi^*\rangle = 0, \quad \langle\xi, \xi^*\rangle = \langle\phi, \psi^*\rangle = 1,$$

all the eigenfunctions are uniquely determined (*e.g.* [7]). We note that

$$\langle\phi, \xi^*\rangle = \langle\xi, \phi^*\rangle = \langle\phi, \phi^*\rangle = 0, \quad \langle\psi, \phi^*\rangle = 1,$$

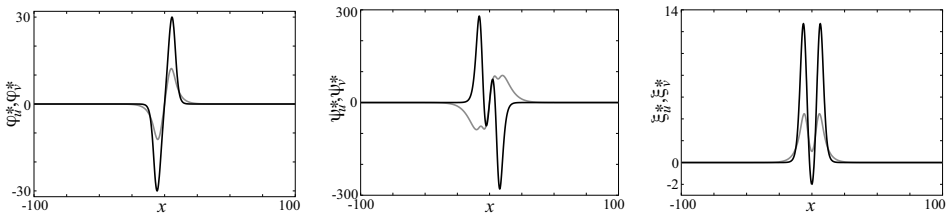

Fig. 12. The profiles of the associated adjoint eigenfunctions of the linearized operator L at the codim 2 point for the Gray-Scott model. u:gray line, v:black line.

hold automatically.

Here $\langle \cdot, \cdot \rangle$ stands for L^2-inner product. Let $E := \mathrm{span}\{S_x, \psi, \xi\}$. Our ansatz is the following

$$\boldsymbol{u} = S(x-p)+q\psi(x-p)+r\xi(x-p)+\zeta^{\dagger}(x-p)+\boldsymbol{w}, \tag{6}$$

where p, q, r are scalar functions of time t; p denotes the location of pulse, q for its velocity, and r the depth of the dimple of splitting. The remaining two terms $\zeta^{\dagger}$ and $\boldsymbol{w}$ belong to $E^{\perp}$. More precisely $\zeta^{\dagger} = q^2\zeta_1 + r^2\zeta_2 + qr\zeta_3 + \eta_1\zeta_4 + \eta_2\zeta_5$ with $\zeta_j \in E^{\perp}$ being determined by

$$\begin{aligned}
L\zeta_1 + \frac{1}{2}F''(S)\psi^2 + \psi_x &= \alpha_1\xi,\\
L\zeta_2 + \frac{1}{2}F''(S)\xi^2 &= \alpha_2\xi,\\
L\zeta_3 + F''(S)\psi\cdot\xi + \xi_x &= \alpha_3\psi + \alpha_3'\phi,\\
L\zeta_4 + \boldsymbol{g}_1(S) &= \alpha_4\xi,\\
L\zeta_5 + \boldsymbol{g}_2(S) &= \alpha_5\xi.
\end{aligned}$$

Here α_j and α_j' are constants satisfying the following equations:

$$\begin{aligned}
&\left\langle \frac{1}{2}F''(S)\psi^2 + \psi_x - \alpha_1\xi,\, \xi^* \right\rangle = 0,\ \left\langle \frac{1}{2}F''(S)\xi^2 - \alpha_2\xi,\, \xi^* \right\rangle = 0,\\
&\langle F''(S)\psi\cdot\xi + \xi_x - \alpha_3\psi,\, \phi^* \rangle = 0,\ \langle F''(S)\psi\cdot\xi + \xi_x - \alpha_3'\phi,\, \psi^* \rangle = 0,\\
&\langle \boldsymbol{g}_1(S) - \alpha_4\xi,\, \xi^* \rangle = 0,\ \langle \boldsymbol{g}_2(S) - \alpha_5\xi,\, \xi^* \rangle = 0.
\end{aligned}$$

Let $\mathcal{L}(X;X)$ be all bounded bilinear operators from X to X. Since $\mathcal{L}(X, \mathcal{L}(X;X))$ is identified with $\mathcal{L}(X\times X;X)$, we represent $(F'(S)\boldsymbol{u})'\boldsymbol{v} \in$

$\mathcal{L}(X;\mathcal{L}(X;X))$ ($\boldsymbol{u}$, $\boldsymbol{v} \in X$) as $F''(S)\boldsymbol{u}\cdot\boldsymbol{v} \in \mathcal{L}(X\times X;X)$, and write $F''(S)\boldsymbol{u}\cdot\boldsymbol{u}$ as $F''(S)\boldsymbol{u}^2$ for simplicity. Third-order derivatives $F'''(S)$ are similarly defined.

Let X^α be the fractional power of space X with respect to the linearized operator L with $\alpha \in (3/4,\ 1)$, and $||\cdot||_\alpha$ denotes the norm of X^α. Then the remainder term $\boldsymbol{w} \in E^\perp$ satisfies the estimate $||\boldsymbol{w}||_\alpha = O\big(|q|^3+|r|^3+|\boldsymbol{\eta}|_2^{3/2}\big)$ where $|\boldsymbol{\eta}|_2 := \sqrt{\eta_1^2+\eta_2^2}$. The proof can be done in a parallel way to [7], however the details will be reported elsewhere. Substituting (6) into (5), we obtain

$$
\begin{aligned}
&-\dot{p}(\phi+q\psi_x+r\xi_x+\zeta_x^\dagger+\boldsymbol{w}_x)+\dot{q}(\psi+\zeta_q^\dagger)+\dot{r}(\xi+\zeta_r^\dagger)+\boldsymbol{w}_t\\
&=L\boldsymbol{w}-qS_x+L\zeta^\dagger+\frac{1}{2}q^2F''(S)\psi^2+qrF''(S)\psi\cdot\xi+\frac{1}{2}r^2F''(S)\xi^2\\
&+qF''(S)\psi\cdot\zeta^\dagger+rF''(S)\xi\cdot\zeta^\dagger+\frac{1}{6}q^3F'''(S)\psi^3+\frac{1}{2}q^2rF'''(S)\psi^2\cdot\xi\\
&+\frac{1}{2}qr^2F'''(S)\psi\cdot\xi^2+\frac{1}{6}r^3F'''(S)\xi^3+\epsilon\chi(x)\boldsymbol{g}_1(S)\\
&+\eta_1\boldsymbol{g}_1(S)+\eta_2\boldsymbol{g}_2(S)+q(\epsilon\chi(x)\boldsymbol{g}_1'(S)+\eta_1\boldsymbol{g}_1'(S)+\eta_2\boldsymbol{g}_2'(S))\psi\\
&+r(\epsilon\chi(x)\boldsymbol{g}_1'(S)+\eta_1\boldsymbol{g}_1'(S)+\eta_2\boldsymbol{g}_2'(S))\xi\\
&+\frac{1}{2}\eta_1^2F''(S)\zeta_4^2+\eta_1\eta_2F''(S)\zeta_4\cdot\zeta_5+\frac{1}{2}\eta_2^2F''(S)\zeta_5^2\\
&+O\big((|q|+|r|+|\boldsymbol{\eta}|_2)(|q|^3+|r|^3+|\boldsymbol{\eta}|_2^{3/2})+|\epsilon|(|q|+|r|+|\boldsymbol{\eta}|_2+|\epsilon|)\big).
\end{aligned}
\tag{7}
$$

Taking the inner product of (7) and $\psi^*(x-p)$, we have

$$
\begin{aligned}
\dot{p}=q-\alpha_3'qr-\epsilon\langle\chi(x)\boldsymbol{g}_1(S),\,\psi^*(x)\rangle\\
+O\big(|q|^3+|r|^3+|\boldsymbol{\eta}|_2^{3/2}+|\epsilon|(|q|+|r|+|\boldsymbol{\eta}|_2+|\epsilon|)\big).
\end{aligned}
$$

Similarly, by taking the inner product of (7) with $\phi^*(x-p)$ and $\xi^*(x-p)$, we have the following two equations.

$$
\begin{aligned}
\dot{q}=&\alpha_3qr+qr^2(-\alpha_3'\langle\xi_x,\,\phi^*\rangle+\langle F''(S)\xi\cdot\zeta_3,\,\phi^*\rangle+\langle F''(S)\psi\cdot\zeta_2,\,\phi^*\rangle\\
&+\frac{1}{2}\langle F'''(S)\psi\cdot\xi^2,\,\phi^*\rangle+\langle\partial_x\zeta_2,\,\phi^*\rangle)\\
&+q^3(\langle F''(S)\psi\cdot\zeta_1,\,\phi^*\rangle+\frac{1}{6}\langle F'''(S)\psi^3,\,\phi^*\rangle+\langle\partial_x\zeta_1,\,\phi^*\rangle)\\
&+\epsilon\langle\chi(x)\boldsymbol{g}_1(S),\,\phi^*\rangle+q(\eta_1\langle\boldsymbol{g}_1'(S)\psi,\,\phi^*\rangle+\eta_2\langle\boldsymbol{g}_2'(S)\psi,\,\phi^*\rangle
\end{aligned}
$$

$$
\begin{aligned}
&+\eta_1\langle F''(S)\psi\cdot\zeta_4,\,\phi^*\rangle+\eta_1\langle\partial_x\zeta_4,\,\phi^*\rangle\\
&+\eta_2\langle F''(S)\psi\cdot\zeta_5,\,\phi^*\rangle+\eta_2\langle\partial_x\zeta_5,\,\phi^*\rangle)\\
&+O\big((|q|+|r|+|\boldsymbol{\eta}|_2)(|q|^3+|r|^3+|\boldsymbol{\eta}|_2^{3/2})+|\epsilon|(|q|+|r|+|\boldsymbol{\eta}|_2+|\epsilon|)\big).\\
\dot r=&\alpha_1q^2+\alpha_2r^2+\epsilon\langle\chi(x)\boldsymbol{g}_1(S),\,\xi^*\rangle+\alpha_4\eta_1+\alpha_5\eta_2\\
&+q^2r(-\alpha_3'\langle\psi_x,\,\xi^*\rangle+\langle F''(S)\xi\cdot\zeta_1,\,\xi^*\rangle+\langle F''(S)\psi\cdot\zeta_3,\,\xi^*\rangle\\
&+\frac{1}{2}\langle F'''(S)\psi^2\cdot\xi,\,\xi^*\rangle+\langle\partial_x\zeta_3,\,\xi^*\rangle)+r^3(\langle F''(S)\xi\cdot\zeta_2,\,\xi^*\rangle\\
&+\frac{1}{6}\langle F'''(S)\xi^3,\,\xi^*\rangle)+r(\eta_1\langle\boldsymbol{g}_1'(S)\xi,\,\xi^*\rangle+\eta_2\langle\boldsymbol{g}_2'(S)\xi,\,\xi^*\rangle\\
&+\eta_1\langle F''(S)\xi\cdot\zeta_4,\,\xi^*\rangle+\eta_2\langle F''(S)\xi\cdot\zeta_5,\,\xi^*\rangle)+\frac{1}{2}\eta_1^2\langle F''(S)\zeta_4^2,\,\xi^*\rangle\\
&+\eta_1\eta_2\langle F''(S)\zeta_4\cdot\zeta_5,\,\xi^*\rangle+\frac{1}{2}\eta_2^2\langle F''(S)\zeta_5^2,\,\xi^*\rangle\\
&+O\big((|q|+|r|+|\boldsymbol{\eta}|_2)(|q|^3+|r|^3+|\boldsymbol{\eta}|_2^{3/2})+|\epsilon|(|q|+|r|+|\boldsymbol{\eta}|_2+|\epsilon|)\big).
\end{aligned}
$$

Using the following notations,

$$
\begin{aligned}
\Gamma_0(p)&=-\int_{-\infty}^{\infty}\chi(x)\boldsymbol{g}_1(S(x-p))\cdot\psi^*(x-p)dx,\\
\Gamma_1(p)&=\int_{-\infty}^{\infty}\chi(x)\boldsymbol{g}_1(S(x-p))\cdot\phi^*(x-p)dx, \qquad (8)\\
\Gamma_2(p)&=\int_{-\infty}^{\infty}\chi(x)\boldsymbol{g}_1(S(x-p))\cdot\xi^*(x-p)dx, \qquad (9)
\end{aligned}
$$

and

$$
\begin{aligned}
M_{11}&=\alpha_3,\\
M_{30}&=\langle F''(S)\psi\cdot\zeta_1,\,\phi^*\rangle+\frac{1}{6}\langle F'''(S)\psi^3,\phi^*\rangle+\langle\partial_x\zeta_1,\,\phi^*\rangle,\\
M_{12}&=\langle F''(S)\xi\cdot\zeta_3,\,\phi^*\rangle+\langle F''(S)\psi\cdot\zeta_2,\,\phi^*\rangle+\frac{1}{2}\langle F'''(S)\psi\cdot\xi^2,\,\phi^*\rangle\\
&\quad+\langle\partial_x\zeta_2,\,\phi^*\rangle-\alpha_3'\langle\xi_x,\,\phi^*\rangle,\\
N_{20}&=\alpha_1,\\
N_{02}&=\alpha_2,\\
N_{21}&=\langle F''(S)\xi\cdot\zeta_1,\,\xi^*\rangle+\langle F''(S)\psi\cdot\zeta_3,\,\xi^*\rangle+\frac{1}{2}\langle F'''(S)\psi^2\cdot\xi,\,\xi^*\rangle\\
&\quad+\langle\partial_x\zeta_3,\,\xi^*\rangle-\alpha_3'\langle\psi_x,\,\xi^*\rangle,
\end{aligned}
$$

$$
\begin{aligned}
N_{03} &= \langle F''(S)\xi\cdot\zeta_2,\,\xi^*\rangle + \frac{1}{6}\langle F'''(S)\xi^3,\xi^*\rangle,\\
\mu_1 &= a_1\eta_1 + a_2\eta_2,\\
\mu_2 &= \alpha_4\eta_1 + \alpha_5\eta_2 + c_1\eta_1^2 + c_2\eta_1\eta_2 + c_3\eta_2^2,\\
\mu_3 &= b_1\eta_1 + b_2\eta_2,\\
a_1 &= \langle \boldsymbol{g}_1'(S)\psi,\,\phi^*\rangle + \langle F''(S)\psi\cdot\zeta_4,\,\phi^*\rangle + \langle \partial_x\zeta_4,\,\phi^*\rangle,\\
a_2 &= \langle \boldsymbol{g}_2'(S)\psi,\,\phi^*\rangle + \langle F''(S)\psi\cdot\zeta_5,\,\phi^*\rangle + \langle \partial_x\zeta_5,\,\phi^*\rangle,\\
b_1 &= \langle \boldsymbol{g}_1'(S)\xi,\,\xi^*\rangle + \langle F''(S)\xi\cdot\zeta_4,\,\xi^*\rangle,\\
b_2 &= \langle \boldsymbol{g}_2'(S)\xi,\,\xi^*\rangle + \langle F''(S)\xi\cdot\zeta_5,\,\xi^*\rangle,\\
c_1 &= \frac{1}{2}\langle F''(S)\zeta_4^2,\,\xi^*\rangle,\\
c_2 &= \langle F''(S)\zeta_4\cdot\zeta_5,\,\xi^*\rangle,\\
c_3 &= \frac{1}{2}\langle F''(S)\zeta_5^2,\,\xi^*\rangle,
\end{aligned}
$$

we can rewrite the above equations as

$$
\begin{cases}
\dot p = q - \alpha_3' qr + \epsilon\Gamma_0(p)\\
\qquad +O\big(|q|^3 + |r|^3 + |\boldsymbol{\eta}|_2^{3/2} + |\epsilon|(|q| + |r| + |\boldsymbol{\eta}|_2 + |\epsilon|)\big),\\
\dot q = \big(M_{30}q^2 + M_{11}r + M_{12}r^2 + \mu_1\big)\,q + \epsilon\Gamma_1(p)\\
\qquad +O\big((|q| + |r| + |\boldsymbol{\eta}|_2)(|q|^3 + |r|^3 + |\boldsymbol{\eta}|_2^{3/2})\\
\qquad\qquad + |\epsilon|(|q| + |r| + |\boldsymbol{\eta}|_2 + |\epsilon|)\big),\\
\dot r = N_{20}q^2 + N_{02}r^2 + N_{21}q^2r + N_{03}r^3 + \mu_3 r + \mu_2 + \epsilon\Gamma_2(p)\\
\qquad +O\big((|q| + |r| + |\boldsymbol{\eta}|_2)(|q|^3 + |r|^3 + |\boldsymbol{\eta}|_2^{3/2})\\
\qquad\qquad + |\epsilon|(|q| + |r| + |\boldsymbol{\eta}|_2 + |\epsilon|)\big).
\end{cases}
\tag{10}
$$

Using the following notation,

$$
\begin{aligned}
&\tilde q = q + Kqr, \qquad \tilde r = r + e_3r^2, \quad dt = (1 + e_1r)d\tau,\\
&\mu_1' = \mu_1 + K\mu_2, \quad \mu_2' = \mu_2, \qquad \mu_3' = \mu_3,
\end{aligned}
$$

where $K = -M_{30}/N_{20}$, $e_1 = -N_{03}/N_{02}$, $e_3 = K - e_1/2 - N_{21}/2N_{20}$, and

$$
\begin{aligned}
&C_0 = M_{11}, \quad C_1 = M_{12} - \frac{N_{02}M_{30}}{N_{20}} - M_{11}\left(\frac{3N_{03}}{2N_{02}} - \frac{M_{30}}{N_{20}} - \frac{N_{21}}{2N_{20}}\right),\\
&C_2 = N_{02}, \quad C_3 = N_{20},
\end{aligned}
$$

we rewrite (10) in the following form:

$$\begin{cases} \dot{p} = \tilde{q} - (K + e_1 + \alpha_3')\tilde{q}\tilde{r} + \epsilon\Gamma_0(p) \\ \qquad +O\big(|\tilde{q}|^3 + |\tilde{r}|^3 + |\boldsymbol{\eta}|_2^{3/2} + |\epsilon|(|\tilde{q}| + |\tilde{r}| + |\boldsymbol{\eta}|_2 + |\epsilon|)\big), \\ \dot{\tilde{q}} = \mu_1'\tilde{q} + C_0\tilde{q}\tilde{r} + C_1\tilde{q}\tilde{r}^2 + \epsilon\Gamma_1(p) \\ \qquad +O\big((|\tilde{q}| + |\tilde{r}| + |\boldsymbol{\eta}|_2)(|\tilde{q}|^3 + |\tilde{r}|^3 + |\boldsymbol{\eta}|_2^{3/2}) \\ \qquad\qquad + |\epsilon|(|\tilde{q}| + |\tilde{r}| + |\boldsymbol{\eta}|_2 + |\epsilon|)\big), \\ \dot{\tilde{r}} = \mu_2' + C_2\tilde{r}^2 + C_3\tilde{q}^2 + \mu_3'\tilde{r} + \epsilon\Gamma_2(p) \\ \qquad +O\big((|\tilde{q}| + |\tilde{r}| + |\boldsymbol{\eta}|_2)(|\tilde{q}|^3 + |\tilde{r}|^3 + |\boldsymbol{\eta}|_2^{3/2}) \\ \qquad\qquad + |\epsilon|(|\tilde{q}| + |\tilde{r}| + |\boldsymbol{\eta}|_2 + |\epsilon|)\big). \end{cases}$$

Replacing

$$\begin{aligned} \rho &= \frac{|C_1|}{C_2}\tilde{q}, \\ \omega &= \frac{|C_1|}{C_2}\left(\tilde{r} + \frac{\mu_3'}{2C_2}\right), \\ \tau &= \frac{C_2^2}{|C_1|}t, \\ \tilde{\mu}_1 &= \frac{C_2^2}{|C_1|}\mu_1', \\ \tilde{\mu}_2 &= \frac{C_2^3}{C_1^2}\mu_2', \\ \theta_1 &= \frac{C_0}{C_2}, \\ \theta_2 &= -\frac{C_3}{C_2}, \\ \tilde{\epsilon} &= \frac{C_1^2}{C_2^3}\epsilon, \end{aligned}$$

and omitting the tildes for simplicity we finally reach the following form

$$\begin{cases} \dot{p} = \dfrac{1}{C_2}\rho - \dfrac{K+e_1+\alpha_3'}{|C_1|}\rho\omega + \dfrac{|C_1|}{C_2^2}\epsilon\Gamma_0(p) \\ \qquad +O\big(|\rho|^3+|\omega|^3+|\boldsymbol{\eta}|_2^{3/2}+|\epsilon|(|\rho|+|\omega|+|\boldsymbol{\eta}|_2+|\epsilon|)\big), \\ \dot{\rho} = \rho(s\mu_1+\theta_1\omega)+\epsilon\Gamma_1(p) \\ \qquad +O\big(|\rho\omega^2|+(|\rho|+|\omega|+|\boldsymbol{\eta}|_2)(|\rho|^3+|\omega|^3+|\boldsymbol{\eta}|_2^{3/2}) \\ \qquad\qquad +|\epsilon|(|\rho|+|\omega|+|\boldsymbol{\eta}|_2+|\epsilon|)\big), \\ \dot{\omega} = \mu_2+\omega^2-\theta_2\rho^2+\epsilon\Gamma_2(p) \\ \qquad +O\big((|\rho|+|\omega|+|\boldsymbol{\eta}|_2)(|\rho|^3+|\omega|^3+|\boldsymbol{\eta}|_2^{3/2}) \\ \qquad\qquad +|\epsilon|(|\rho|+|\omega|+|\boldsymbol{\eta}|_2+|\epsilon|)\big), \end{cases} \tag{11}$$

where $s = \mathrm{sign}[C_1] = \pm 1$.

The qualitative behaviors of (2) can be classified into eight categories depending on the signs of θ_1, θ_2 and s, however, for definiteness, we assume the following, which is one of interesting cases in applications.

We impose the following assumption.

(S5) We assume that $C_1 \neq 0$, and C_2, θ_1, $\theta_2 > 0$.

It is known that (S5) is numerically confirmed at the codim 2 point of the saddle-node and drift bifurcations for (3) and (4). For instance, using the eigenfuctions depicted in Fig. 12, we have $\theta_1 \approx 0.93$, $\theta_2 \approx 0.11$.

We fix $|\mu_1|$ to be sufficiently small and take $\mu_2 = O(|\mu_1|^{2-\nu})$ and $\epsilon = O(|\mu_1|^{2-\nu})$ $(2/3 < \nu < 1)$. Then, in the first equation of (11), $O(\rho)$ becomes the leading order, and we discard the terms higher than ρ. In the second and third equations of (11), we consider the regime where $\rho = O(|\mu_1|^{1-\nu})$ and $\omega = O(|\mu_1|^{1-\nu})$, and discard the terms of the order higher than $|\mu_1|^2$. Then the principal part of (11) is

$$\begin{cases} \dot{p} = \rho/C_2, \\ \dot{\rho} = \rho(s\mu_1+\theta_1\omega)+\epsilon\Gamma_1(p), \\ \dot{\omega} = \mu_2+\omega^2-\theta_2\rho^2+\epsilon\Gamma_2(p). \end{cases} \tag{12}$$

Loosely speaking, here ρ stands for the pulse velocity, and ω corresponds to the amplitude of the splitting. It should be noted that the finite dimensional system (12) has a universal form, namely it depends only on the singularities and heterogeneities. In particular, recalling (8) and (9), (12) preserves the same form even for general $\chi(x)$ such as spatially periodic and random functions.

5. Dynamics of the principal part of ODEs

5.1. Homogeneous case

For $\epsilon = 0$, i.e., the homogeneous case, the second and third equations of (12) are independent of p. It is therefore sufficient to study the following system:

$$\begin{cases} \dot{\rho} = \rho(s\mu_1 + \theta_1\omega), \\ \dot{\omega} = \mu_2 + \omega^2 - \theta_2\rho^2. \end{cases} \tag{13}$$

The equilibrium points with $\rho = 0$ correspond to the standing pulse solutions, and those with $\rho \neq 0$ correspond to the traveling pulse solutions. There exist an unstable standing pulse solution

$$E_1^+ : (\rho, \omega) = (0, +\sqrt{-\mu_2}),$$

and a stable one up to the drift bifurcation point

$$E_1^- : (\rho, \omega) = (0, -\sqrt{-\mu_2}).$$

These two standing pulses merge at $\mu_2 = 0$ and form the saddle-node bifurcation point as shown in Fig. 13(a). E_1^- loses its stability at $\mu_2 = -\mu_1^2/\theta_1^2$ and a drift bifurcation occurs there. At $\mu_2 = -\mu_1^2/\theta_1^2$, stable equilibrium points with $\rho \neq 0$

$$E_2^\pm : (\rho, \omega) = \left(\pm\sqrt{(\mu_2 + \mu_1^2/\theta_1^2)/\theta_2},\ -s\mu_1/\theta_1\right) \tag{14}$$

bifurcate from E_1^-. Note that E_2^+ (respectively E_2^-) with $\rho > 0$ ($\rho < 0$) represents a right (left)-going traveling pulse solution. It is easy to verify by simple computation that $E_2^\pm$ is locally stable, i.e., the bifurcation is supercritical. Fig. 13(a) shows the schematic bifurcation diagram for (13) with $s\mu_1 > 0$ being fixed. Fig 13(b) shows the phase portraits of (13) as μ_2 is varied. From Fig 13(b), it is easy to see that the unstable manifolds emanating from $E_1^\pm$ are connected to $E_2^\pm$. In the sequel we mainly work in Region II and III (see Fig. 13) where $E_2^\pm$ exist.

5.2. Heterogeneous case

The heterogeneous perturbations $\Gamma_1(p)$ and $\Gamma_2(p)$ (see (8) and (9)) are functions of p and are independent of ϵ, μ_1 and μ_2. Typical profiles for the Gray-Scott model (3) with the hetrogeneity $\chi(x) = 1/(1 + \exp(-\gamma x))$ are shown in Fig. 14. They are negative-valued functions. Γ_1 converges to 0 as

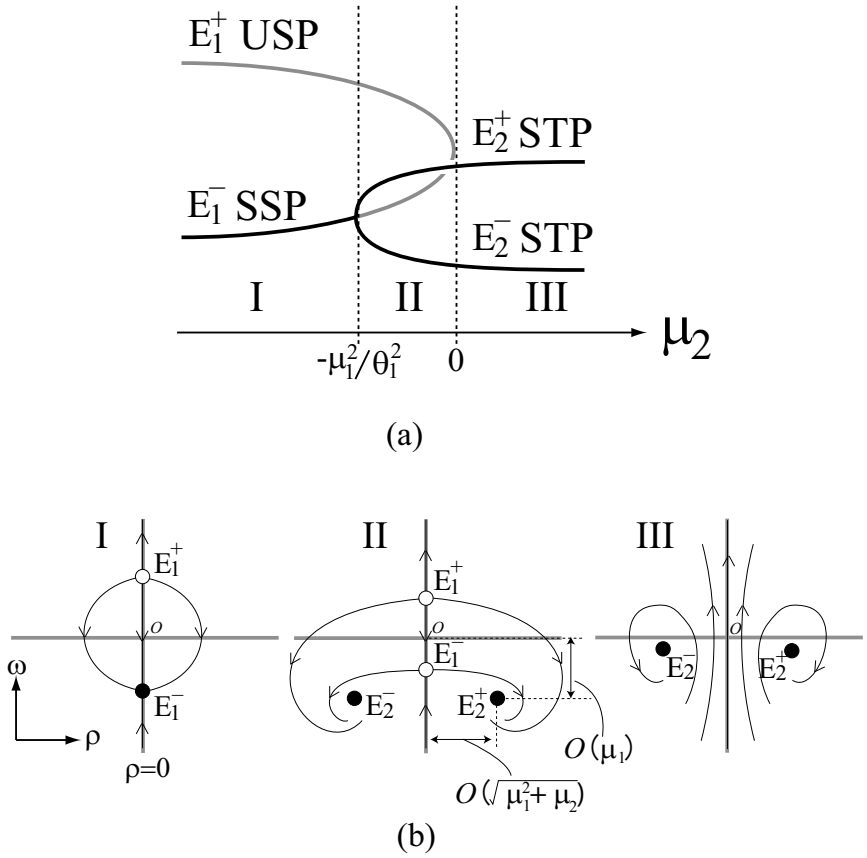

Fig. 13. Schematic bifurcation diagram (Fig. a) and Phase portrait (Fig. b) for (13) with fixed $s\mu_1 > 0$. Here SSP and USP are stable and unstable standing pulse respectively. STP is stable traveling pulse. Gray line corresponds to existence region of STP, and dark gray line is for SSP. Black and white circles indicate stable and unstable solution respectively. In Region II, unstable manifolds emanating from $E_1^{\pm}$ connect to $E_2^{\pm}$.

$p \to \pm\infty$ because $S(x)$ is an even function and ϕ^* is an odd function. Γ_2 converges to $\bar{\Gamma}_2 < 0$ as $p \to +\infty$ because ξ^* is an even function. In general $\Gamma_1(p)$ and $\Gamma_2(p)$ depend on the profiles of $\chi(x)$ as well as model system and do not always take negative values, however the above asymptotic behaviors are guaranteed for single jump heterogeneity, since they come from the symmetry of eigenfunctions. Hereafter, for definiteness, we assume the

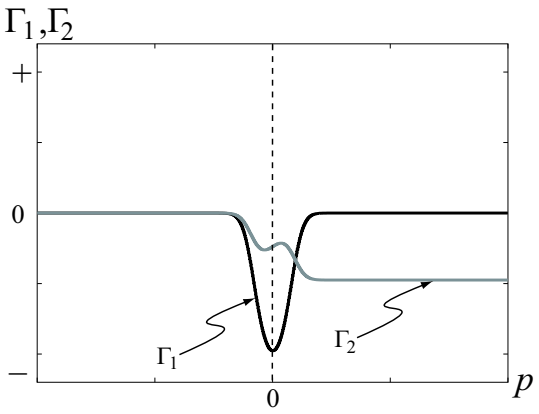

Fig. 14. The profiles of the heterogeneous perturbations for jump type: black line for Γ_1 and gray line for Γ_2, which is obtained numerically for the Gray-Scott model.

following for $\Gamma_1(p)$ and $\Gamma_2(p)$.

(S6) $\Gamma_1(p)$ is a negative function which decays exponentially to 0 as $p \to \pm\infty$, and it has the minimum at $p = 0$. $\Gamma_2(p)$ is a negative function which decays exponentially to 0 as $p \to -\infty$ and approaches a negative constant $\bar{\Gamma}_2$ as $p \to +\infty$.

First note that the system (12) does not have equilibria from (S6), however they can be defined asymptotically for $|p| \to +\infty$ in the projected (ρ, ω)-space thanks to the limiting properties of the heterogeneity $\lim_{p\to+\infty} \Gamma_1(p) = 0$ and $\lim_{p\to+\infty} \Gamma_2(p) = \bar{\Gamma}_2 < 0$. The equilibrium points for $p \to +\infty$ in (ρ, ω)-space are given by

$$\widetilde{E}_1^{\pm}\colon (\rho, \omega) = \Big(0, \pm\sqrt{-\mu_2 - \epsilon\bar{\Gamma}_2}\Big),$$

$$\widetilde{E}_2^{\pm}\colon (\rho, \omega) = \Big(\pm\sqrt{(\mu_2 + \epsilon\bar{\Gamma}_2 + \mu_1^2/\theta_1^2)/\theta_2},\ -\mu_1/\theta_1\Big).$$

Since $\lim_{p\to-\infty} \Gamma_1(p) = 0$ and $\lim_{p\to-\infty} \Gamma_2(p) = 0$, the traveling pulse solutions for $p \to -\infty$ remains the same as in the homogeneous case, i.e., $E_2^{\pm}$ (see (14)).

Our problem can be formulated as follows. Starting from E_2^+ for $p = -\infty$ and trace the behavior of its orbit as $t \to \infty$, namely characterize the behavior of the one-dimensional unstable manifold emanating from E_2^+

in 3D phase space. Our analysis in this paper is, however, focused on the behavior of the orbits starting from the initial data $(p_0, \rho_0, \omega_0) = (p(0), \rho(0), \omega(0))$ with some conditions, where p_0 is sufficiently negative large, $\rho(0) > 0$, and $\omega(0) < 0$.

The onset of splitting is the aftereffect of the unstable manifold of the saddle-node bifurcation of the stationary pulse (Fig. 4) and may be expected to occur when the orbit is driven by heterogeneous terms to a point near $\rho = 0$ of Fig. 13(b) III, or the unstable manifold of E_1^+ of Fig. 13(b) II. In order to have a splitting, it is necessary for ω to grow in time. In view of the third equation of (12), it is clear that the sign of

$$\lambda(t) := \mu_2 - \theta_2\rho^2(t) + \epsilon\Gamma_2(p(t))$$

is important for such a growth. In fact, if $\lambda(t) < 0$ holds for all $t > 0$, then splitting does not occur provided that $\omega(0) < 0$ and $p(0)$ is sufficiently small and negative. Based on the above discussions, we give the definitions of penetration, splitting, and rebound in terms of ODEs.

Definition 5.1 When (ρ, ω) converges to $\widetilde{E}_2^+$ as $t \to +\infty$, the dynamics is called penetration.

Definition 5.2 When $\omega > \delta$ for some finite δ, the dynamics is called splitting.

Since we study (12) in the neighbourhood of codim 2 point, the size of (ρ, ω) is small and hence the constant δ in the above definition can be taken to be arbitrary finite number.

Definition 5.3 When (ρ, ω) converges to E_2^- as $t \to +\infty$, the dynamics is called rebound.

Fig. 15 shows the phase diagram for (12) with respect to μ_2 and ϵ. It essentially inherits the original PDE dynamics shown in Fig. 10 and Fig. 11. There exist three regions: penetration, splitting and the rebound, and splitting region exists in between the penetration and the rebound regions. Note that, since Γ_1 and Γ_2 are negative, the heterogeneity makes ρ and ω decrease. That is, if the initial condition is close to E_2^+, then $\rho = O(\sqrt{\mu_2 + \mu_1^2/\theta_1^2})$ for arbitrary t (see the proofs of Lemmas in the sequel).

We now consider two typical transitions among penetration, splitting, and rebound depicted by two arrows in Fig. 15, namely μ_1 is fixed to be

small and μ_2 and ϵ are varied satisfying the following linear relation for some constants a and b to be chosen later.

$$\mu_2 = a\epsilon + b \tag{15}$$

In other words ϵ (height of the jump) is the control parameter and μ_2 is slave to it according to (15).

Our goal is to prove Propositions 5.1 and 5.2 and we prove a sequence of Lemmas for that purpose.

Lemma 5.1 *If there exists the time T such that for $p < +\infty$ $\rho(T) = 0$, then $\rho(t) < 0$ for $t > T$.*

Proof. From the second equation of (12), $\dot{\rho} < 0$ at $\rho = 0$ for $p(t) < +\infty$. □

For a given initial condition (p_0, ρ_0, ω_0) with $\rho(0) > 0$, the parameter ϵ belongs to one of the following sets. It should be noted from Lemma 5.1 that once $\rho(t)$ changes its sign from positive to negative, it remains negative.

$$\begin{aligned}
\mathcal{E}^+(a,\, b; \hat{\mu}_1) :=& \{\hat{\epsilon} \in \mathbb{R} \mid \liminf_{t\to\infty} \rho(t) > 0 \text{ for all } t \geq 0 \\
& \qquad \text{for } \epsilon = \hat{\epsilon},\ \mu_2 = a\hat{\epsilon} + b,\ \mu_1 = \hat{\mu}_1\} \\
\mathcal{E}^0(a,\, b; \hat{\mu}_1) :=& \{\hat{\epsilon} \in \mathbb{R} \mid \rho(t) > 0 \text{ for all } t > 0 \text{ and } \liminf_{t\to\infty} \rho(t) = 0 \\
& \qquad \text{for } \epsilon = \hat{\epsilon},\ \mu_2 = a\hat{\epsilon} + b,\ \mu_1 = \hat{\mu}_1\} \\
\mathcal{E}^-(a,\, b; \hat{\mu}_1) :=& \{\hat{\epsilon} \in \mathbb{R} \mid \rho(t) = 0 \text{ at a finite positive } t = T < \infty \\
& \qquad \text{for } \epsilon = \hat{\epsilon},\ \mu_2 = a\hat{\epsilon} + b,\ \mu_1 = \hat{\mu}_1\}
\end{aligned}$$

Lemma 5.2 *Take $p(0) < 0$, $\rho(0) > 0$ and $\omega(0) < 0$. Suppose $\mathcal{E}^+$ and $\mathcal{E}^-$ are not empty and $|\omega(t)|$ is uniformly bounded for all $t > 0$, then $\mathcal{E}^0$ is not empty. Moreover if $\mathcal{E}^0 \neq \emptyset$, then $p(t) \to \infty$ for $\epsilon \in \mathcal{E}^0$.*

Proof. First we show that $\mathcal{E}^0 \neq \emptyset$ by using open-closed argument. Since $\mathcal{E}^+$ and $\mathcal{E}^-$ are not empty, there exist $\epsilon^+ \in \mathcal{E}^+$ and $\epsilon^- \in \mathcal{E}^-$. We can assume without loss of generality that $\epsilon^+ < \epsilon^-$, since $\mathcal{E}^+ \cap \mathcal{E}^- = \emptyset$ and therefore either $\epsilon^- < \epsilon^+$ or $\epsilon^+ < \epsilon^-$ holds. $[\epsilon^+,\, \epsilon^-]$ is obviously a closed set, but $\widetilde{\mathcal{E}}^+ := [\epsilon^+,\, \epsilon^-] \cap \mathcal{E}^+$ is not closed as will be shown below. Take any $\epsilon' \in \widetilde{\mathcal{E}}^+$. Then $\liminf_{t\to\infty} \rho(t)$ has a non-zero positive value, it is clear that $p(t) \to \infty$ as $t \to \infty$. Recalling that there exists a unique hyperbolic equilibrium point $\widetilde{E}_2^+$ in the positive ρ-region, it follows from the boundedness of $\omega(t)$ and

the exponentially decaying property of heterogeneous terms that the orbit converges to $\widetilde{E}_2^+$ in (ρ, ω)-plane. Using the continuous dependency of the orbit on the initial data and parameters, there exists a δ-neighbourhood of $\epsilon = \epsilon'$ such that any orbit starting from this neighbourhood also converges to $\widetilde{E}_2^+$, which shows $\liminf_{t\to\infty} \rho(t) > 0$ and hence $\widetilde{\mathcal{E}}^+$ is not a closed set. On the other hand, take any $\epsilon'' \in \widetilde{\mathcal{E}}^- := [\epsilon^+, \epsilon^-] \cap \mathcal{E}^-$, then $\rho(T) = 0$ at some finite $t = T$, therefore, from the continuous parametric dependency of solution, there exists a δ-neighbourhood of $\epsilon = \epsilon''$ such that the orbit with ϵ being in this neighbourhood satisfy $\rho(T') = 0$ for some T' close to T, i.e., it belongs to $\tilde{\mathcal{E}}^-$. Hence $\widetilde{\mathcal{E}}^-$ is not a closed set. Therefore we conclude that $\mathcal{E}^0$ is not empty because $[\epsilon^+, \epsilon^-]$ can not be covered by the union of two open sets $\widetilde{\mathcal{E}}^+$ and $\widetilde{\mathcal{E}}^-$.

The final part of the Lemma, namely the property of $p(t) \to \infty$ for the parameters in $\mathcal{E}^0$ can be proved by contradiction, namely there exists $\bar{p} < \infty$ such that $\sup_t p = \bar{p}$ holds, although $\rho(t) > 0$ for all $t > 0$. Noting that $p(0) \le p(t) \le \bar{p}$ holds thanks to $\rho(t) > 0$, we see that the negative quantity $\tilde{\Gamma}_1 := \max_{p(0)\le p\le\bar{p}} \Gamma_1(p)$ is well-defined. Since $\rho(t) > 0$ and $p(t) < \bar{p}$, it is easy to verify that $\rho(t) \to 0$ as $t \to \infty$ in view of the first equation of (12). Since $|\omega|$ is uniformly bounded, we can find some $t = t'$ at which $\rho(s\mu_1 + \theta_1\omega) < -\epsilon\tilde{\Gamma}_1/2$ is satisfied leading to the inequality

$$\dot{\rho} < \frac{\epsilon\tilde{\Gamma}_1}{2} < 0, \quad t \ge t'$$

from the second equation of (12). This contradicts to the fact that we choose the parameter from $\widetilde{\mathcal{E}}^0$, because the above inequality implies that $\rho(t)$ reaches 0 in finite time. □

Lemma 5.3 *Suppose that* $s\mu_1 > 0$, $-\mu_1^2/\theta_1^2 < \mu_2 \le 0$, $p(0) < \infty$ *and* $\omega(0) < 0$. *If* $\epsilon = 0$ *and* $\rho(0) > 0$, *then* $(\rho(t), \omega(t))$ *converges to* $E_2^+ (= \widetilde{E}_2^+)$. *If* $\epsilon = |\mu_1|^{2-\nu}$ *and* $\rho(0) = 0$, *then* $(\rho(t), \omega(t))$ *converges to* E_2^-.

Proof. In view of the phase space Fig. 13(b), it is clear that the orbit tends to E_2^+ when $\epsilon = 0$, $\rho(0) > 0$ and $\omega < 0$.

In order to prove the convergence to E_2^- for the case of $\epsilon = |\mu_1|^{2-\nu}$ with $\rho(0) = 0$, we show that $\rho(t)$ and $\omega(t)$ is uniformly bounded and $\rho(t)$ is bounded away from zero, which turns out to be sufficient for the purpose combined with the hyperbolicity of the equilibrium point E_2^-. Also, from Lemma 5.1, note that $\rho(t)$ is negative for all t.

First we show that there exist constants $t_0 > 0$ and $\underline{\rho} < 0$ such that $\underline{\rho} < \rho(t)$ for $t > t_0$. From (12) and Lemma 5.1

$$\dot{\rho} > s\mu_1\rho + \epsilon\Gamma_1(p) > s\mu_1\rho + \epsilon\bar{\Gamma}_1, \quad t \geq 0. \tag{16}$$

where $\bar{\Gamma}_1 = \inf_{-\infty<p<p(0)} \Gamma_1(p)$. Assume that $\rho(t)$ reaches $\overline{\rho} = -|\mu_1|^{(1+\nu')/2}$ $(0 < \nu' < 1-\nu)$ at $t = t_1 > 0$. From (16) and $\rho(t_1) = -|\mu_1|^{(1+\nu')/2}$, we have

$$\rho(t) > -\frac{\epsilon\bar{\Gamma}_1}{s\mu_1} + \left(\frac{\epsilon\bar{\Gamma}_1}{s\mu_1} - |\mu_1|^{(1+\nu')/2}\right)\exp\bigl(s\mu_1(t-t_1)\bigr), \quad t \geq t_1. \tag{17}$$

Note that the second term of the right-hand side of (17) is negative. Expanding the exponential term into Taylor series up to 1st order and recalling that $2/3 < \nu < 1$ and $0 < \nu' < 1-\nu$, we obtain the following inequality from (17)

$$\rho(t) > -|\mu_1|^{(1+\nu')/2} + G(\mu_1), \tag{18}$$

where $G(\mu_1) := \bigl(\epsilon\bar{\Gamma}_1/s\mu_1 - |\mu_1|^{(1+\nu')/2}\bigr)\exp(s\mu_1|\mu_1|^{-(1+\nu')/2})$ and is of order $O(|\mu_1|^{3/2-\nu-\nu'/2})$ for $t < t_2 := t_1 + |\mu_1|^{-(1+\nu')/2}$. Let $\underline{\rho}$ be defined to be the quantity of the right-hand side of (18), then, as long as $\rho \in (\underline{\rho}, \overline{\rho})$, we have the following inequality from (12).

$$\mu_2 + \omega^2 - \theta_2\underline{\rho}^2 + \epsilon\Gamma_2(p) < \dot{\omega} < \mu_2 + \omega^2 - \theta_2\overline{\rho}^2 + \epsilon\Gamma_2(p), \quad t_1 \leq t \leq t_2 \tag{19}$$

Since $\underline{\rho}$ and $\overline{\rho}$ is of order $|\mu_1|^{(1+\nu')/2}$ and by using the assumptions for μ_2 and ϵ as well as recalling the basic hypothesis $\omega = O(|\mu_1|^{1-\nu})$ when deriving the principal part of ODEs (12), we can find appropriate positive constants $\overline{c}$ and $\underline{c}$ such that

$$-\underline{c}|\mu_1|^{(1+\nu')/2} < \omega(t_2) < -\overline{c}|\mu_1|^{(1+\nu')/2}. \tag{20}$$

Here we used the fact that the solution of $\dot{\omega} = \omega^2 - k$ can be expressed by the following.

$$\frac{1}{2\sqrt{k}}\left[\log\left|\frac{\omega(T)-\sqrt{k}}{\omega(T)+\sqrt{k}}\right| - \log\left|\frac{\omega(0)-\sqrt{k}}{\omega(0)+\sqrt{k}}\right|\right] = T$$

Combining (12), (18) with (20), we have

$$\begin{aligned}\dot{\rho}(t_2) &= \rho(t_2)(s\mu_1 + \theta_1\omega(t_2)) + \epsilon\Gamma_1(p(t_2)) \\ &= \theta_1\rho(t_2)\omega(t_2) + O(|\mu_1|^{2-\nu}) > 0,\end{aligned}$$

which shows that even if $\dot{\rho}$ is negative when ρ reaches $\overline{\rho}$, the sign of $\dot{\rho}$ is changed to positive before $t = t_2$. Moreover for $t \geq t_1$, since we have $\dot{\rho} = \theta_1\rho\omega + O(|\mu_1|^{2-\nu}) > 0$ for $\rho \in (\underline{\rho}, \overline{\rho})$, the term $\rho\omega(\sim |\mu_1|^{1+\nu'})$ dominates the right-hand side. Thus we can conclude that $\rho(t) > \underline{\rho}$ holds for all time.

Next we show that there exist $\rho' < 0$ and $t' > 0$ such that $\rho(t) < \rho'$ for $t > t'$. First we show that $\lim_{t\to\infty} p = -\infty$ holds by contradiction. Assume $\underline{p} := \inf_{t>0} p(t) > -\infty$ holds. From Lemma 5.1, $\rho(t) < 0$ for all $t > 0$. Since $\underline{p} > -\infty$, $\lim_{t\to\infty} \rho = 0$. This follows that $\lim_{t\to\infty} \dot{\rho} \to \epsilon\Gamma(\underline{p}) < 0$ from (12). Therefore $p < \underline{p}$ holds, which contradicts to $\lim_{t\to\infty} \rho = 0$, i.e., $\lim_{t\to\infty} p = -\infty$ holds.

Now we are ready to prove that $\rho(t)$ has a negative upper bound ρ'. Suppose that $\rho(t)$ does not have such a bound, (ρ, ω) necessarily converge to E_1^- owing to $\lim_{t\to\infty} p \to -\infty$. Moreover it is easily seen that $\lim_{t\to\infty} |\Gamma_j(p)| = 0$ $(j = 1, 2)$ and $\lim_{t\to\infty} \omega = -\sqrt{-\mu_2}$ holds from the third equation of (12), therefore it follows from $-\mu_1^2/\theta_1^2 < \mu_2 < 0$ that $\lim_{t\to\infty}(s\mu_1 + \theta_1\omega) = (s\mu_1 - \theta_1\sqrt{-\mu_2}) > 0$. This implies from the second equation of (12) that $\dot{\rho} < 0$ in finite time, which leads to the contradiction to the above convergence to E_1^-. Hence it holds that there exist ρ' and $t' > 0$ such that $\underline{\rho} < \rho(t) < \rho' < 0$ for $t > t'$. Combining this with the former part of the proof, we can conclude that $\rho \in (\underline{\rho}, \rho')$ for all $t > t'$, which leads to the convergence of (ρ, ω) to nondegenerate stable equilibrium point E_2^- as $t \to \infty$. □

Lemma 5.4 *Let T_1 and T_2 be the times when p_1 and p_2 reaches at $\ell > p_j(0)$ $(j = 1, 2)$ respectively. Suppose that $p_1(0) = p_2(0)$, $0 \leq \dot{p}_1(t) \leq \dot{p}_2(t)$ $(\forall t \geq 0)$ and $T_2 < +\infty$. Then*

$$\int_0^{T_1} \Gamma_1(p_1)dt \leq \int_0^{T_2} \Gamma_1(p_2)dt \tag{21}$$

holds. If $\dot{p} = c$ $(c > 0)$ with $p(0) = \ell_1$ and $p(T) = \ell_2$, then

$$\int_0^T \Gamma_1(p)dt = \frac{1}{c}\int_{\ell_1}^{\ell_2} \Gamma_1(l)dl. \tag{22}$$

Proof. Since $T_2 < +\infty$, the right side of (21) is finite. If $T_1 = +\infty$, the left side of (21) is $-\infty$. Hence (21) holds. If $T_1 < +\infty$, (21) is obvious. □

Lemma 5.5 *Let $\nu' > 1 - \nu/2$, $\epsilon = |\mu_1|^{2-\nu}$, $p(0) = -\ell$, $\rho(0) = O(|\mu_1|^{\nu'})$ and $\omega(0) < 0$. Suppose $\omega(t) \le 0$ for all $t > 0$. Then, for sufficiently small $|\mu_1|$, $\rho(t)$ is monotonically decreasing as long as $p(t) \in [-\ell, \ell]$.*

Proof. When $\rho(t) \ge 0$ and $\omega(t) \le 0$,

$$\begin{aligned}\frac{d\rho}{dt} &\le s\mu_1\rho(t) + \epsilon\Gamma_1 \\ &\le s\mu_1\rho(t) + \epsilon\tilde{\Gamma}_1,\end{aligned}$$

where $\tilde{\Gamma}_1 = \max_{p\in[-\ell,\ell]} \Gamma_1(p)$. Since $s\mu_1\rho(0) = O(|\mu_1|^{1+\nu'})$ and $\epsilon = |\mu_1|^{2-\nu}$, $\rho(t)$ is monotonically decreasing as long as $p(t) \in [-\ell, \ell]$ for sufficiently small $|\mu_1|$. □

Lemma 5.6 *Let $\nu' > 1 - \nu/2$, $\epsilon = |\mu_1|^{2-\nu}$, $p(0) = -\ell$, $\rho(0) = O(|\mu_1|^{\nu'})$ and $\omega(0) < 0$. Suppose $\omega(t) \le 0$ for all $t > 0$. Then $\rho(T) = 0$ at $T = O(|\mu_1|^{\nu+\nu'-2})$ and $p(t) \le \ell$ for $t \le T$ by taking sufficiently small $|\mu_1|$.*

Proof. Since $\omega(t) \le 0$, from the second equation of (12) and Lemma 5.5

$$\frac{d\rho(t)}{dt} \le s\mu_1\rho(0) + \epsilon\tilde{\Gamma}_1, \tag{23}$$

as long as $p \in [-\ell, \ell]$ where $\tilde{\Gamma}_1 = \max_{p\in[-\ell,\ell]} \Gamma_1(p) < 0$. By integrating both sides of (23) from $t = 0$ to T, we have

$$\rho(T) - \rho(0) \le s\mu_1\rho(0)T + \epsilon\tilde{\Gamma}_1 T.$$

Since $\rho(T) = 0$,

$$T \le \frac{-\rho(0)}{\epsilon\tilde{\Gamma}_1 + s\mu_1\rho(0)} = O(|\mu_1|^{\nu+\nu'-2}),$$

and $p(T) < \rho(0)T = O(|\mu_1|^{\nu+2\nu'-2}) < \ell$ holds for sufficiently small $|\mu_1|$. □

Lemma 5.6 implies $\mathcal{E}^- \neq \emptyset$ for $\epsilon = |\mu_1|^{2-\nu}$, $p(0) = -\ell$, $\rho(0) = O(|\mu_1|^{\nu'})$ and $\omega(0) < 0$ provided that μ_2 (or equivalently a and b in (15)) can be chosen appropriately so that $\omega(t) \le 0$ holds for all t. Noting that if $\mu_2 \le 0$, then $\lambda(t) \le 0$ holds, therefore we have $\omega(t) \le 0$ for all $t > 0$ (recall the remark after the assumption (S6)). The following proposition is a direct consequence of this fact.

Proposition 5.1 *Let $\nu' > 1-\nu/2$, $a = 0$, $b \in [-\mu_1^2/\tilde{\theta}_1^2, 0]$ $(\tilde{\theta}_1 > \theta_1)$, $p(0) = -\ell$, $\rho(0) = O(|\mu_1|^{\nu'})$ and $\omega(0) < 0$. Then the dynamics changes from penetration to rebound as ϵ is increased from 0 to $|\mu_1|^{2-\nu}$ for sufficiently small $|\mu_1|$.*

Proof. First we note that E_2^+ exists for $\mu_2 = b \in [-\mu_1^2/\tilde{\theta}_1^2, 0]$. Since $\mu_2 \le 0$, $\lambda(t) \le 0$ holds for all $t > 0$, i.e., $\omega(t) \le 0$ holds. From Lemma 5.6, there exists $T < \infty$ such that $\rho(T) = 0$ for $\epsilon = O(|\mu_1|^{2-\nu})$. From Lemma 5.3, $(\rho(t), \omega(t))$ converges to E_2^-, i.e., rebound occurs.

On the other hand, from Lemma 5.3, $(\rho(t), \omega(t))$ converges to $\widetilde{E}_2^+$ for $\epsilon = 0$. Therefore the dynamics changes from penetration to rebound as ϵ is increased from 0 to $|\mu_1|^{2-\nu}$ for sufficiently small $|\mu_1|$. □

We formulate the following lemma to prove Proposition 5.2.

Lemma 5.7 *Let $\nu' > 1-\nu/2$, $\nu'' \le 1-\nu/2$, $0 < a < \bar{\Gamma}_2$, $b = 0$, $\epsilon = |\mu_1|^{2-\nu}$, $p(0) = -\ell$, $\rho(0) = |\mu_1|^{\nu'}$ and $\omega(0) = -|\mu_1|^{\nu''}$. Then $\rho(t)$ reaches zero in a finite time for sufficiently small $|\mu_1|$.*

Proof. Let $\epsilon = |\mu_1|^{2-\nu}$. From the third equation of (12)

$$\frac{d\omega(t)}{dt} \le \mu_2 + \omega^2(t). \tag{24}$$

Let T be time when $\omega(t)$ attains 0. From (24) and $\omega(0) = -|\mu_1|^{\nu''}$,

$$T \ge \frac{1}{\sqrt{\mu_2}} \tan^{-1}\left(\frac{|\omega(0)|}{\sqrt{\mu_2}}\right) \ge \frac{|\omega(0)|}{\sqrt{\mu_2}} = O(|\mu_1|^{\nu''+\nu-2}) \tag{25}$$

holds where we use $\tan^{-1}(x) \ge x$ $(0 < x \ll 1)$. Since $\nu'' \le 1-\nu/2$, there exist $c' \in \mathbb{R}$ such that $T \ge c'|\nu_1|^{-1+\nu/2}$. From the second equation of (12) and Lemma 5.5,

$$\frac{d\rho}{dt} \le s\mu_1\rho(0) + \epsilon\tilde{\Gamma}_1. \tag{26}$$

Since $\omega(t) \le 0$ for $t \in [0, T]$, by integrating both hand sides of (26) from $t = 0$ to T, we have

$$\rho(T) \le \rho(0) + s\mu_1\rho(0)T + \epsilon\tilde{\Gamma}_1 T. \tag{27}$$

From $\epsilon = c|\mu_1|^{2-\nu}$ and (25), the third term of the right hand side of (27) becomes leading order for sufficiently small $|\mu_1|$, that is $\rho(T) < 0$. Therefore $\rho(t)$ attains 0 in finite time while $\omega(t) \le 0$. □

Proposition 5.2 *Let $\nu' > 1-\nu/2$, $\nu'' \le 1-\nu/2$, $0 < a < \bar{\Gamma}_2$, $b = 0$, $\epsilon = |\mu_1|^{2-\nu}$, $p(0) = -\ell$, $\rho(0) = |\mu_1|^{\nu'}$ and $\omega(0) = -|\mu_1|^{\nu''}$. Then the dynamics changes from penetration to splitting as ϵ is increased from 0 to $|\mu_1|^{2-\nu}$ for sufficiently small $|\mu_1|$.*

Proof. It is obvious that the penetration occurs for $\epsilon = 0$, i.e., $\mathcal{E}^+ \neq \emptyset$. From Lemma 5.7, ρ changes its sign at $\epsilon = |\mu_1|^{2-\nu}$, i.e., $\mathcal{E}^- \neq \emptyset$. From Lemma 5.2, $\mathcal{E}^0 \neq \emptyset$. Since $p(t)$ tends to ∞, $\lambda(t)$ tends to $\mu_2 + \epsilon\bar{\Gamma}_2 = \epsilon(a - \bar{\Gamma}_2) > 0$ for $\epsilon \in \mathcal{E}^0$. Therefore the third equation of (12) gives

$$\frac{d\omega}{dt} \approx \omega^2 + \epsilon(a - \bar{\Gamma}_2) \ge \epsilon(a - \bar{\Gamma}_2).$$

Therefore ω attains 1 at $t \le O(1/\epsilon)$, i.e. splitting occurs for $\epsilon \in \mathcal{E}^0$. □

As is shown in Fig. 15, the ODE dynamics seems to reflect the essential part of the original PDE dynamics at least qualitatively. The Proposition 5.1 and Proposition 5.2 show that it is the case for some appropriate parameter regime. The transition from penetration to rebound for the ODE dynamics (12) is depicted in Fig. 16 for $\mu_1 = -0.1$, $\mu_2 = 0.006$, $s = -1$, $\theta_1 = 0.93$, $\theta_2 = 0.11$, $C_2 = 0.85$.

Remark 5.1 (Dependency on the slope) The slope of the heterogeneity is controlled by γ of the function $\chi(x)$. Recalling the definition of Γ_1 (*see* (8)), it is easy to verify that $\Gamma_1 \to 0$ as $\gamma \to 0$, therefore the pulse can go across the high barrier when its solpe becomes gentle even if the pulse rebounds for the steeper case as in Fig. 18.

6. Concluding remarks

We considered the pulse dynamics for the heterogeneous media where there is only one abrupt change in spatial direction. Three different types of behaviors for traveling pulses, namely penetration, splitting, and rebound, are observed depending on the height of the jump. Using the pulse-dynamics approach, PDE dynamics can be reduced to study the ODE dynamics as in Sections 4 and 5. It was clarified that the codim 2 singularity (drift+saddle-node) for the standing pulse is a kind of organizing center which actually controls the output when the pulse meet the heterogeneity. Our analysis can be easily extended to the bump type if the size of the bump is large enough compared with that of the pulse, in particular, for the Gray-Scott model (3)

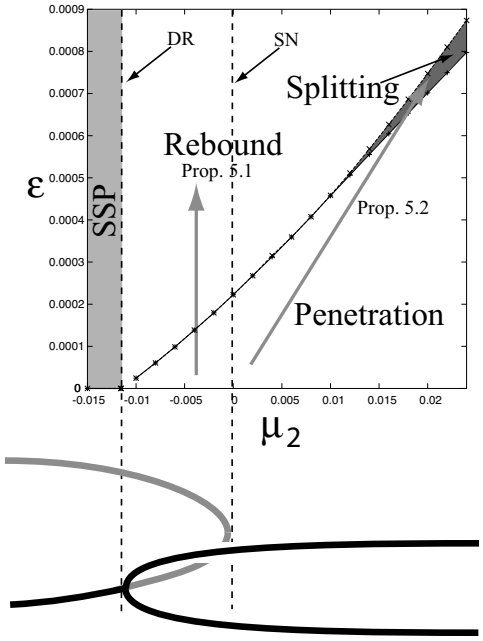

Fig. 15. Phase diagram of (12) for the Gray-Scott model. Here $\mu_1 = -0.1$, $s = -1$, $\theta_1 = 0.93$, $\theta_2 = 0.11$, $C_2 = 0.85$. SSP stands for stable standing pulse, DR means drift bifurcation, and SN presents saddle-node bifurcation.

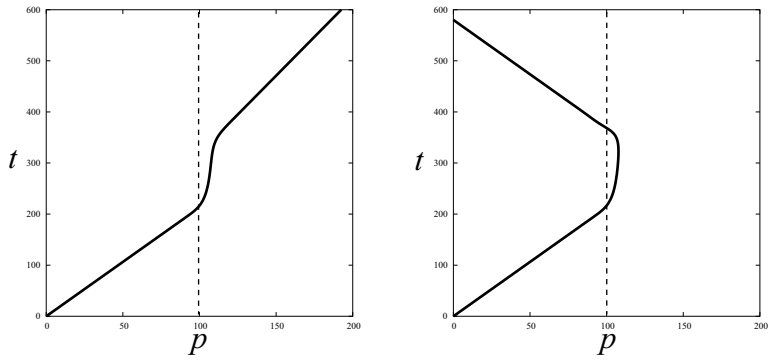

Fig. 16. Numerical simulations of (12) with $\mu_1 = -0.1$, $\mu_2 = 0.006$, $s = -1$, $\theta_1 = 0.93$, $\theta_2 = 0.11$, $C_2 = 0.85$. These parameter values correspond to the Gray-Scott model. The left figure shows penetration ($\epsilon = 3.3524 \times 10^{-4}$), and the right figure illustrates rebound ($\epsilon = 3.3525 \times 10^{-4}$).

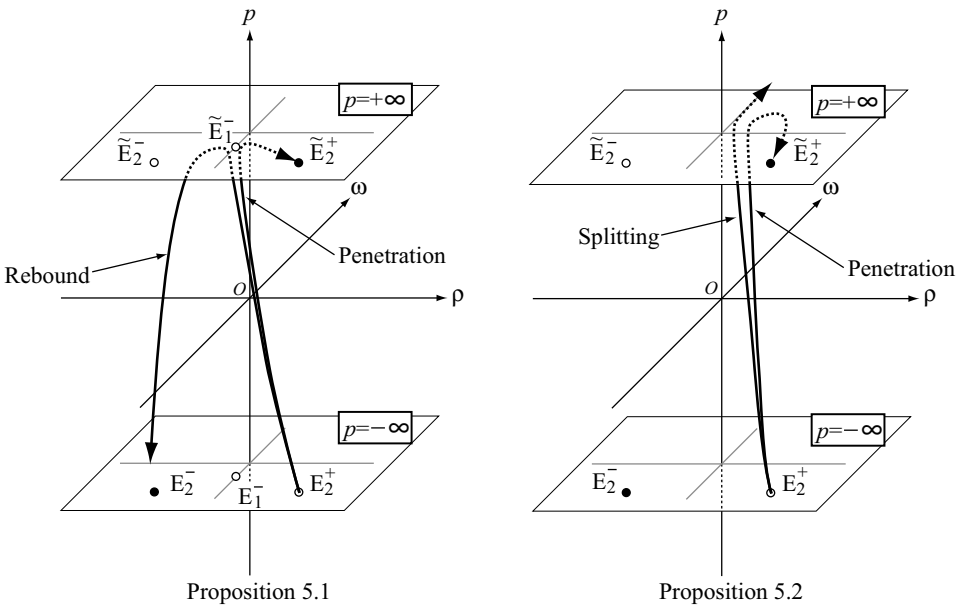

Fig. 17. Schematic phase portrait for (12). Black and white circles indicate stable and unstable stationary solutions respectively.

case, penetration always occur at the jump-down point, i.e., k is decreased as x is increased (see Fig. 10), therefore the behavior of the pulse is basically determined by the jump-up point. It should be remarked for the bump case that there appears another localized standing pulse located at the center of the bump which plays a role as a separator for penetration, splitting, and rebound. Existence of such a separator can be shown by noting that $\epsilon\Gamma_1$ (see (8)) becomes an odd function, and therefore it has a zero point at the center. Furthermore the ODE formula (12) remains valid for any heterogeneity including periodic and random media. In fact, for spatially periodic heterogeneity, there are at least three representative classes.

- Long wave limit: the period of heterogeneity is much longer than the width of the pulse.
- Short wave limit: the period of heterogeneity is much shorter than the width of the pulse.
- Resonant case: they are comparable.

The first one is essentially equivalent to the case of very gentle slope men-

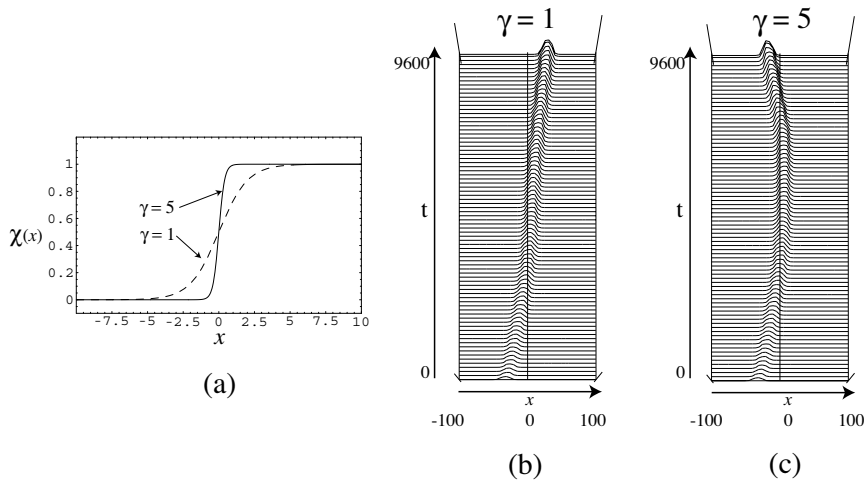

Fig. 18. When the slope of heterogeneity becomes less steep, the pulse can penetrate. The profile of $\chi(x)$ is illustrated by (a). For $f = 0.026$, $k = 0.05652$, $\epsilon = 3.2 \times 10^{-5}$, the pulse penetrate when $\gamma = 1$ (see (b)), however it turns back when $\gamma = 5$ (see (c)).

tioned in Remark 5.1, namely the traveling pulse does not feel the heterogeneity and can penetrate it. Recalling the definition of Γ_1, if χ oscillates rapidly, Γ_1 converges weakly to zero, therefore pulse can also penetrate for the short wave limit. The most delicate and interesting case is the third case. It is known that a variety of dynamics including spatio-temporal chaos is observed numerically [37] for comparable case, in fact, loosely speaking, the dynamics is very close to that of pendulum with external time-periodic kicks. The detailed analysis is currently investigated and will be reported elsewhere.

Acknowledgment The authors of this paper would like to thank Prof. Ei and Prof. Ikeda for fruitful comments. Special thanks go to the anonymous referees for valuable comments and suggestions. This work was partially supported by the Grant-in-Aid for Scientific Research (A) 16204008, the Grant-in-Aid for Young Scientists (B) 18740050 and Core Research for Evolutional Science and Technology (CREST), Japan Science and Technology Agency (JST): Creation of Novel Nano-material/system Synthesized by Self-organization for Medical Use.

References

[1] Astrov Y.A. and Purwins H.-G., *Plasma spots in a gas discharge system*: *Birth, scattering and formation of molecules*. Phys. Lett. A (5-6) **283**, 349–354.

[2] Argentina M., Coullet P. and Mahadevan L., *Colliding Waves in a Model Excitable Medium*: *Preservation, Annihilation, and Bifurcation*. Phys. Rev. Lett. **79** (1997), 2803–2806.

[3] Bär M., Eiswirth M., Rotermund H.-H. and Ertl G., *Solitary-wave phenomena in an excitable surface reaction*. Phys. Rev. Lett. **69** (1992), 945–948.

[4] Bode M., Liehr A.W., Schenk C.P. and Purwins H.-G., *Interaction of dissipative solitons: particle-like behaviour of localized structures in a three-component reaction-diffusion system*. Physica D **161** (2002), 45–66.

[5] Ei S.-I., *The motion of weakly interacting pulses in reaction diffusion systems*. J. Dyn. Diff. Eqs. (1) **14** (2002), 85–137.

[6] Ei S.-I. and Ikeda H., *Personal communication*.

[7] Ei S.-I., Mimura M. and Nagayama M., *Pulse-pulse interaction in reaction-diffusion systems*. Physica D **165** (2002), 176–198.

[8] Ei S.-I., Nishiura Y. and Ueda K.-I., 2^n*-splitting or edge splitting–A manner of splitting in dissipative systems–*. Jpn. J. Inds. Appl. Math. (2) **18** (2001), 181–205.

[9] Gray P. and Scott S.K., *Autocatalytic reactions in the isothermal, continuous stirred tank reactor -oscillations and instabilities in the system* $A + 2B \to 3B$; $B \to C$. Chem. Eng. Sci. **39** (1984), 1087–1097.

[10] Gutman M., Aviram I. and Rabinovitch A., *Pseudoreflection from interface between two oscillatory media*: *Extended driver*. Phys. Rev. E **69** (2004), 016211-1–016211-8.

[11] Gutman M., Aviram I. and Rabinovitch A., *Abnormal frequency locking and the function of the cardiac pacemaker*. Phys. Rev. E **70** (2004), 037202-1–037202-4.

[12] Hayase Y. and Ohta T., *Self-replicating pulses and Sierpinski gaskets in excitable media*. Phys. Rev. E **62** (2000), 5998–6003.

[13] Ikeda H. and Mimura M., *Wave-Blocking Phenomena in Bistable Reaction-Diffusion Systems*. SIAM J. Appl. Math. (2) **49** (1989), 515–538.

[14] Kepper P. de, Perraud J.-J., Rudovics B. and Dulos E., *Experimental study of stationary Turing patterns and their interaction with traveling waves in a chemical system*. Int. J. Bifur. Chaos (5) **4** (1994), 1215–1231.

[15] Kinezaki N., Kawasaki K., Takasu F. and Shigesada N., *Modeling biological invasions into periodically fragmented environments*. Theoretical Population Biology, **64** (2003), 291–302.

[16] Kobayashi R., Ohta T. and Hayase Y., *Self-organized pulse generator in a reaction-diffusion system*. Phys. Rev. E **50** (1994), R3291-R3294.

[17] Krischer K. and Mikhailov A., *Bifurcation to Traveling Spots in Reaction-Diffusion Systems*. Phys. Rev. Lett. **73** (1994), 3165–3168.

[18] Kuznetsov Y.A., *Elements of Applied Bifurcation Theory Second edition*. Springer, 1998.

[19] Lee K.J., McCormick W.D., Pearson J.E. and Swinney H.L., *Experimental observation of self-replicating spots in a reaction-diffusion system*. Nature **369** (1994), 215–218.

[20] Merkin J.H., Petrov V., Scott S.K. and Showalter K., *Wave-Induced Chemical Chaos*. Phys. Rev. Lett. **76** (1996), 546–549.

[21] Nishiura Y. and Ueyama D., *A skeleton structure of self-replicating dynamics*. Physica D **130** (1999), 73–104.

[22] Nishiura Y., Teramoto T. and Ueda K.-I., *Scattering and separators in dissipative systems*. Phys. Rev. E **67** (2003), 056210-1–056210-7.

[23] Nishiura Y., Teramoto T. and Ueda K.-I., *Dynamic transitions through scattors in dissipative systems*. Chaos (3) **13** (2003), 962–972.

[24] Nishiura Y., *Far-from-equilibrium dynamics*. Chap. 6 AMS, (2003).

[25] Nishiura Y., Teramoto T. and Ueda K.-I., *Scattering dynamics of traveling pulses near singularities*. preprint.

[26] Oertzen A. von, Mikhailov A.S., Rotermund H.H. and Ertl G., *Subsurface Oxygen in the CO Oxidation Reaction on Pt(110): Experiments and Modeling of Pattern Formation*. J. Phys. Chem. B. (25) **102** (1998), 4966–4981.

[27] Ohta T., *Pulse dynamics in a reaction-diffusion system*. Physica D **151** (2001), 61–72.

[28] Pauwelussen J.P., *Nerve impulse propagation in a branching nerve system: a simple model*. Physica D **4** (1981), 67–88.

[29] Pauwelussen J.P., *One way traffic of pulses in a neuron*. J. Math. Biology **15** (1982), 151–171.

[30] Pearson J.E., *Complex patterns in a simple system*. Science **261** (1993), 189–192.

[31] Petrov V., Scott S.K. and Showalter K., *Excitability, wave reflection, and wave splitting in a cubic autocatalysis reaction-diffusion system*. Phil. Trans. Roy. Soc. Lond. Series A **347** (1994), 631–642.

[32] Press W.H., Teukolsky S.A., Vetterling W.T. and Flannery B.P., *Numerical Recipes in C*. Cambridge Univ. Press, 1988.

[33] Purwins H.-G., Astrov Yu.A. and Brauer I., *Proceedings of the Fifth Experimental Chaos Conference*. edited by M. Ding, W.L. Ditto, L.M. Pecora and M.L. Spano, World-Scientific, Singapore, 2001, pp. 3–13.

[34] Reynolds W.N., Ponce-Dawson S. and Pearson J.E., *Self-replicating spots in reaction-diffusion systems*. Phys. Rev. E **56** (1997), 185–198.

[35] Schenk C.P., Or-Guil M., Bode M. and Purwins H.-G., *Interacting Pulses in Three-Component Reaction-Diffusion Systems on Two-Dimensional Domains*. Phys. Rev. Lett. **78** (1997), 3781–3784.

[36] Teramoto T., Ueda K.-I. and Nishiura Y., *Phase-dependent output of scattering process for traveling breathers*. Phys. Rev. E **69** (2004), 056224-1–056224-8.

[37] Ueyama D., *Personal communication*.

[38] Xin J., *Front Propagation in Heterogeneous Media*. SIAM Rev. (2) **42** (2000), 161–230.

[39] Zimmermann M.G., Firle S.O., Natiello M.A., Hildebrand M., Eiswirth M., Bär M., Bangia A.K. and Kevrekidis I.G., *Pulse bifurcation and transition to spatiotemporal chaos in an excitable reaction-diffusion model*. Physica D **110** (1997), 92–104.

Y. Nishiura
Research Institute for Electronic Science
Hokkaido University
Kita-ku N12 W6, Sapporo
Hokkaido, 060-0812 Japan

Y. Oyama
Research Institute for Electronic Science
Hokkaido University
Kita-ku N12 W6, Sapporo
Hokkaido, 060-0812 Japan
E-mail: oyama@nsc.es.hokudai.ac.jp

K. Ueda
Research Institute for Mathematical Sciences
Kyoto University